12-2018

Computational Infrared Spectroscopy of HNO Beyond the Double Harmonic Approximation

Harkiran Kaur Dhah
University of Tennessee

To the Graduate Council:

I am submitting herewith a dissertation written by Harkiran Kaur Dhah entitled "Computational Infrared Spectroscopy of HNO Beyond the Double Harmonic Approximation." I have examined the final electronic copy of this dissertation for form and content and recommend that it be accepted in partial fulfillment of the requirements for the degree of Doctor of Philosophy, with a major in Chemistry.

Robert Hinde, Major Professor

We have read this dissertation and recommend its acceptance:

Charles Collins, Brian Long, Sharani Roy

Accepted for the Council:

Dixie L. Thompson

Vice Provost and Dean of the Graduate School

(Original signatures are on file with official student records.)

Computational Infrared Spectroscopy of HNO Beyond the Double Harmonic Approximation

A Dissertation Presented for the
Doctor of Philosophy
Degree
The University of Tennessee, Knoxville

Harkiran Kaur Dhah
December 2018

Acknowledgements

To my parents, Mohinder and Ravinder, you taught me at an early age the importance of education. It was with your love, encouragement, and understanding that I was able to pursue my doctoral degree and reach this point in my life. I love you with all of my heart and I can never thank you enough for all that you have done for me.

To my brothers, Sunny and Jimmy, it is wonderful to think back to our childhood and see how our many shared experiences helped us grow into the adults we are today. My earning a higher degree follows your example, and I have been so lucky to have both of you to look up to.

To my many cousins and aunts and uncles, you have always been very close to me and for that I am very thankful. I thank you for all of the love and support that you have provided me throughout the years.

To my fiancé, Jonathan, although we began our relationship before, most of our relationship has been during graduate school. Thank you for your constant encouragement through it all. If not for your continued belief in me, my many nights of staying up late to finish assignments and study for exams would not have been possible. I thank you for your love and support which showed me that I had the capability to earn my doctorate. I look forward to beginning our married life together and knowing the same support will be provided.

To my friends and colleagues throughout graduate school, while we were all going through our own stresses, I am glad we found close friendships along the way. I would especially like to thank my friends Andrea, Ashleigh, Dan, Eric, Gavin, Heather, Jenn, Josh, Matt, Paul, Rachel, Randi, and one of my best friends, James, who made work a place I always looked forward to going. While we leave for our different professional careers I look forward to our friendships continuing and to meet again to catch up where we left off.

And very importantly, to Dr. Hinde, thank you for accepting me in your research group and for your mentorship for the past several years. Your wisdom, patience, and good heart helped me greatly to achieve this goal.

Abstract

This work explores, for the first time, the calculation of HNO molar absorptivities using methods that go beyond the double harmonic approximation. Accurate molar absorptivities of HNO are essential for the kinetic interpretation of recent experiments that studied tunneling-mediated chemistry of H + NO reactions at low temperatures. This work will show that the double harmonic approximation for computing molar absorptivities is not sufficient to obtain accurate molar absorptivities for HNO. Since the only published molar absorptivities for HNO are computed using the double harmonic approximation, they cannot be used to interpret the experimental data.

First, we compute the molar absorptivity values using the double harmonic approximation with several combinations of basis sets and theories. With the double harmonic approximation, we also calculate the vibrational frequency shifts with isotopic substitutions of the individual atoms within the HNO molecule. After comparing double harmonic results to experimental results, we consider extensions to this approximation. By including anharmonic effects, we first consider electrical anharmonicity alone, and then consider the combination of electrical and mechanical anharmonicity. With the inclusion of both forms of anharmonicity, the molar absorptivity values change greatly from the double harmonic molar absorptivity values. Lastly effects of mechanical coupling are investigated. Results from this investigation encourage future work that

would include mechanical coupling, and also consider electrical coupling, in accurate calculations of HNO molar absorptivities.

This work will show that large basis sets are required for the theoretical calculation of the molar absorptivities of HNO, and that the double harmonic approximation is unreliable for this molecule. In particular, the NH stretching mode is very anharmonic. The computed isotopic shifts in the vibrational frequencies of HNO are found to be very sensitive to the way in which electron-electron correlation is treated. This indicates that very high level electron correlation models may be important for accurate theoretical studies of HNO. Finally, the extension beyond the double harmonic approximation and treatment with anharmonic effects are proven to be extremely valuable in describing the true mechanical and electrical properties of HNO.

Table of Contents

List of Tables

List of Figures

Chapter 1

Introduction

1.1 Importance of Nitrosyl Hydride

The nitrosyl hydride molecule, HNO, was first experimentally observed in 1958 (Dalby 1958). This molecule over the past century has been studied experimentally and theoretically due to its involvement in several areas. The breakdown of stratospheric ozone has been suggested to involve HNO as an intermediate (Patrick and Golden 1984). In 1977, HNO was first reported to be detected from interstellar emissions, which was important to the astrochemical community as it confirmed the first detection of the NO bond in interstellar molecules (Ulich, Hollis et al. 1977). HNO has also been expected to have an application towards heart failure treatment (Miranda, Katori et al. 2005). Ongoing research of this molecule continues.

HNO molecules can be produced from reactions of hydrogen radicals with NO molecules. As shown in Table 1.1.1 (Bozkaya, Turney et al. 2012), these reactants can result in four possible products, which are ^{1}HNO, ^{3}HNO, ^{1}NOH, and ^{3}NOH. All of these product formations are exothermic, so the resultant molecule formed is lower in energy than that of the hydrogen radical and NO molecule from which they were produced. As seen from this table, all of the products but ^{1}HNO have a classical energy barrier that must be overcome by the reactants before the products can be formed. To surpass this barrier, the reactants must have enough kinetic energy, and this energy increases with the temperature of the environment. The distribution of kinetic energies at a specific temperature is described by the Maxwell-Boltzmann distribution.

Table 1.1.1. Listing of all four possible products from the reaction of a hydrogen radical with a NO radical, and literature values of exothermicity from formation of products and the activation energy for each product. (Bozkaya, Turney et al. 2012)

Product	Exothermicity (kcal/mol)	Activation Energy (kcal/mol)
^{1}HNO	47.48	None
^{3}HNO	29.03	3.38
^{1}NOH	5.25	2.63
^{3}NOH	21.3	12.37

1.2 Experimental Background

David Anderson from the University of Wyoming Department of Chemistry studies low temperature reaction kinetics. Reactions between hydrogen atoms and several co-reagents are being studied within a *para*-hydrogen matrix at extremely low temperatures between 1 and 5 Kelvin. By studying the several hydrogen atom reactions that occur with these co-reagents at such low temperatures, Anderson aims to gain an understanding of the reaction rate and mechanism through which these reactions take place. Spectroscopic analysis aids in understanding these reactions (Ruzi and Anderson 2015).

Para-hydrogen molecules have a rotational state of j = 0 at ground state, whereas the rotational state of *ortho*-hydrogen molecules is j = 1 at ground state. The rotational quantum number, j, is determined from the nuclear spin. The antisymmetric *para* nuclear spin state is composed of the two hydrogen atoms in the H_2 molecule with opposite spins, resulting in j of 0, 2, 4, and other even state numbers. The symmetric *ortho* nuclear spin state is composed of the two hydrogen atoms in the H_2 molecule with the same spins, resulting in j of 1, 3, and other odd state numbers. A *para*-hydrogen molecule with j of 0 is the lowest in energy, and hence is the most stable hydrogen spin state. Nuclear spin state conversions between *ortho* and *para* are forbidden except in the presence of a substance that can act as a converter. Anderson utilizes matrix isolation of *para*-hydrogen complexes at low temperatures.

Anderson has been studying the kinetics of low temperature reactions, particularly at 1.8 and 4.3 K, of nitric oxide (NO) radical dopants in a predominately

para-hydrogen crystal matrix after a portion of the crystal is irradiated with ultraviolet light. The NO radicals that were struck with this light then dissociate into N and O atoms. Each of these atoms react with their neighboring hydrogen molecules to produce, as one of the products, a hydrogen atom.

An *ortho-para* converter is used to insure 99.97% of the hydrogen gas molecules are in the *para*-hydrogen state. The NO-doped solid *para*-hydrogen crystal is prepared by codeposition of both NO and *para*-hydrogen gas onto a BaF_2 substrate. Ultraviolet light is passed through the doped crystal at a wavelength of 193 nm, producing the nitrogen and oxygen atoms that then react with H_2 molecules to produce hydrogen atoms. The hydrogen atoms then diffuse through the crystal. Electron Spin Resonance (ESR) spectroscopy studies have concluded that this hydrogen atom diffusion occurs in solid *para*-hydrogen through reactive tunneling (Kumada, Sakakibara et al. 2002, Kumada 2003). Quantum tunneling refers to reactions that occur by passing through a potential energy barrier. This type of reaction neglects the requirement of having or supplying enough energy to overcome the potential energy barrier. The hydrogen atom diffusion through the *para*-hydrogen matrix involves an exchange reaction between the *para*-hydrogen molecules and the hydrogen atoms.

$$H + H_2 \rightarrow H_2 + H$$
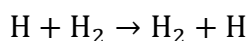
The energy barrier between the reactants and products in the above reaction is ~10 kcal mol^{-1} (Ruzi and Anderson 2015). At Anderson's experimental temperature of 4.3 K, integration of the tail of the Maxwell-Boltzmann distribution shows that less than 1

hydrogen atom out of 10^{250} atoms will have 10 kcal mol^{-1} of kinetic energy (Benderskii, Goldanskii et al. 1993), therefore the reaction must occur through tunneling.

Anderson studies the bimolecular reactions that occur with the hydrogen atoms and the NO dopants. Completing these studies at low temperatures allows immobilization of certain species, thus preventing reactions from taking place between these species and others within the matrix, or reactions between the same species. Once a hydrogen radical is in proximity to a NO dopant, a reaction occurs. As expected from Table 1.1.1, HNO is a product. Although this reaction also takes place at the same low temperatures, this reaction occurs without tunneling, as this is a barrierless exothermic reaction.

$$H + NO \rightarrow HNO$$
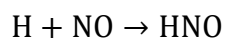
Surprisingly, the other product that is formed is ^{3}NOH. Due to the high energetic barrier to produce ^{3}NOH and the low temperatures at which Anderson performs his experiments, the production of ^{3}NOH occurs through tunneling.

A fourier transform infrared (FTIR) spectrometer records spectra at the onset of irradiation and at subsequent times for a period of up to 5 hours. The three peaks in the ^{1}HNO spectra represent the NH stretch, NO stretch, and molecular bend vibrations. The FTIR peak intensities are shown to increase over time following photolysis, indicating a growth in the amount of ^{1}HNO and ^{3}NOH produced since the initial production of the nitrogen and oxygen atoms. If the peak intensities can be converted to concentrations, then Anderson's group can follow the growth rate of the ^{1}HNO and ^{3}NOH products

during the experiment. An accurate growth rate is required for kinetic analysis of this reaction.

1.3 Theoretical Background

Once the doped *para*-hydrogen crystal is irradiated, HNO production is initiated. To calculate the kinetics of the HNO production, accurate absorption coefficients are needed that represent the absorbance per unit concentration for this molecule. The pattern of growth of HNO over time using previously calculated absorption coefficients indicates a first-order reaction (Lee 1993). The exact concentration of HNO can be calculated from any of the HNO FTIR peaks by considering the integrated absorption coefficients (ε) and the absorbances (A) of the peaks, where $A = \log_{10}(I_0/I)$, where I_0 is the light intensity initially striking the crystal and I is the light intensity remaining after passing through the crystal. V_0 has a set value of 23.16 cm^3 mol^{-1} which represents the molar volume of the solidified *para*-hydrogen at the temperature of liquid helium, and l is the path length the infrared light travels through the crystal.

$$[\text{HNO}] = \frac{2.303 \int \log_{10}(I_0/I) d\tilde{v}}{\varepsilon l} V_0 (10^6)$$

The only previously published integrated absorption coefficients available prior to this work were reported in 1993 by T.J. Lee (Lee 1993), using a computational approximation called the double harmonic approximation and using a comparatively small basis set as to those easily available today. A basis set is a set of basis functions to be used to model the electronic wave function of an atom. The specific basis set used by Lee was the triple-zeta double polarized (TZ2P) basis set. The double harmonic

7

approximation treats potential energy functions as second-order polynomials to describe each vibrational motion. Additionally, the double harmonic approximation also treats dipole moment functions as first-order polynomials to describe each vibrational motion. These simplifications greatly simplify the work required to obtain molar absorptivity values.

When Anderson's group uses these absorption coefficients, the resultant HNO concentration determined from the NH stretch vibration differs from that calculated from the molecular bend vibration by a factor of two. This means that the HNO concentrations produced in Anderson's experiments are still too uncertain to allow a kinetic analysis of the reaction. This large disagreement of the HNO concentration makes it essential to explore absorption coefficients computed with larger basis sets and with calculations that are beyond the double harmonic approximation.

1.4 Overview of Work

The following chapters will detail our work to obtain more accurate absorption coefficients than those currently available. All of this work was completed through *ab initio* calculations and through code written in Maple. All of the calculations in this dissertation were for singlet HNO.

In chapter 2 we will detail our work testing the double harmonic approximation, which was completed through *ab initio* calculations with use of modern basis sets, as well as with different levels of theories. Chapter 3 will include results of the double harmonic approximation and analysis of these results. Harmonic frequencies were

obtained for the HNO molecule, along with harmonic frequencies following substitution of different isotopes of the atoms within the molecule for analysis of the kinetic isotope effect. Using these vibrational frequencies and further *ab initio* work, we obtained harmonic potential energy functions and dipole moment functions to describe each vibrational motion. This allowed us to compute the double harmonic molar absorptivity of each vibrational motion. The measurement by which our values were determined accurate was by comparison to experimental work by Anderson.

In chapter 4 we will detail our work for extending potential energy functions and dipole moment functions beyond the double harmonic approximation to see the effects of including anharmonicity to compute molar absorptivites. After this we will consider including coupling between different vibrational motions to see the effect of more than one vibrational mode influencing the molecule at one time.

Chapter 5 includes details of how to further extend this work. Lastly, a summary of the importance of this work and the results of this work will be provided.

Chapter 2

Double Harmonic

Approximation

2.1 Introduction

Prior calculations of molar absorptivity for the vibrational motions of HNO have treated the molecule using only the double harmonic approximation (Lee 1993). This approximation is frequently used to avoid extra computational cost, but for certain molecules the vibrational behavior requires an extension to the double harmonic approximation to describe more accurately behaviors such as the potential energy change and dipole moment change with each vibrational motion, which in turn has an effect on the molar absorptivity. The double harmonic approximation assumes non-coupling of vibrational modes; that is that each vibration has an independent effect on the molecule. The number of vibrational modes for a nonlinear molecule is (3N-6), where N represents the total number of atoms within the molecule. For the nonlinear HNO molecule there are a total of three vibrational modes, labeled q1, q2, q3, in order of decreasing frequency. Each vibrational mode is described by the collective displacements of the H, N, and O atoms. Three geometric parameters are affected by these normal modes, which are the NH bond length, NO bond length, and the HNO bond angle.

The potential energy function of the molecule is dependent on each of the normal modes. In the double harmonic approximation, each potential energy function is assumed to be symmetric and quadratic in the minimum vicinity of the potential energy. The dipole moment function of the molecule is also dependent on each of the normal modes, and in the double harmonic approximation each dipole moment function is assumed to be a linear function of the normal mode coordinates. As will be discussed in

section 2.2, the molar absorptivity computed within the double harmonic approximation requires components from accurate potential energy functions and dipole moment functions. The calculations for the optimization of HNO, as well as for potential energies and dipole moments of the HNO structures, will be completed through *ab initio* molecular orbital theory calculations. The *ab initio* optimization adjusts the geometrical parameters, such as bond lengths and bond angle, calculating the potential energy after each adjustment, and repeats this process though several iterations until a minimal energy is found.

2.1.1 Optimization

To compute the optimized geometry of HNO and the potential energy of this optimal geometry, which corresponds to the minimal energy along the potential energy curve, an optimized *ab initio* calculation was completed. Geometric optimization of HNO is simplified by treating this 2-dimensional molecule in the (x, y) plane. Past work by Bozkaya studied the energetics of HNO and its isomer, NOH, and the kinetics of the HNO $\leftrightarrow$ NOH isomerization (Bozkaya, Turney et al. 2012). Our work initialized the placement of each atom in the HNO structure by using Bozkaya's computed geometry, although we used a different basis set than used by Bozkaya, and we converted this geometry to coordinates of each of the H and O atoms while placing the N atom at the origin and the NO bond along the x-axis. Optimization of this initial geometry yielded optimal bond lengths, bond angle, and potential energy.

2.1.2 Basis Sets and Theory

In order to test the dependence of our optimization and the work that followed the optimization on the basis set, two basis sets were used. Our work employed augmented correlation-consistent polarized valence basis sets, specifically aug-cc-pVTZ and aug-cc-pVQZ. The basis set for each atom is made up of a number of Gaussian functions and when implemented for each atom in our molecule, it provides a close approximation to the molecular orbitals. Increasing from triple zeta to quadruple zeta raises the number of basis functions significantly, and this large increase of basis functions results in a considerable increase in computational cost. Augmentation of these basis sets adds diffuse functions to more accurately describe the outer regions of the atoms, which is necessary for the correct description of weak bonds, such as the NH bond in the HNO molecule, as well as for correct calculations of certain properties such as dipole moment.

Several computational theories were used in our calculations, specifically Hartree-Fock (HF), second-order Møller-Plesset theory (MP2), and coupled-cluster theories, including CCSD and CCSD(T). The Hartree-Fock theory treats the electrons of an orbital in an average manner and neglects instantaneous interactions between electrons in other orbitals known as electron-electron correlation. This neglect of electron correlation enables the Hartree-Fock method to conserve computational cost, and this method is correct to the first order of energies. Møller-Plesset includes an approximate treatment of electron correlation using perturbation theory, and MP2 is correct to the second order in the perturbation. Coupled-cluster models excitation of

electrons into virtual orbitals using the cluster operator, and includes increasing amounts of electron correlation. CCSD treats single and double excitations, and CCSD(T) includes, in addition, a non-iterative treatment of triple excitations, which reduces computational cost significantly compared to the CCSDT method. The mean absolute error of standard dipole moment calculations of relatively small molecules was found to be 0.16 D with Hartree Fock, 0.048 D with MP2, 0.025 D with CCSD, and less than 0.01 D with CCSD(T) (Bak, Gauss et al. 2000). A similar pattern is observed for the mean absolute error of bond lengths and bond angles of relatively small molecules that contain atoms from the second row of the period table (Coriani, Marchesan et al. 2005).

2.2 Molar Absorptivity and the Double Harmonic Approximation

The formula for calculating the molar absorptivity (A) of a specific vibrational mode considers both its vibrational frequency (v) and the absorption intensity (G_{ji}), where i and j represent the initial and final vibrational levels, respectively (Cohen, et al. 2008).

$$A = \frac{G_{ji}v}{16.60540}$$

G_{ji} is a function of the transition dipole moment (M_{ji}). The transition dipole moment, squared, is made up of a sum over the Cartesian components of the integral of the dipole moment operator $\mu_{\rho}(q)$, squared, over vibrational levels i and j.

$$G_{ji} = \frac{8\pi^3}{3hc_0(4\pi\varepsilon_0)}\left|M_{ji}\right|^2 = 41.6238\left|M_{ji}\right|^2$$

$$|M_{ji}|^2 = \sum_\rho |\langle i|\mu_\rho(q)|j\rangle|^2$$

The double harmonic approximation assumes equal spacing between each energy level and limits transitions to between the ground state, $i = 0$, and the first excited energy level, $j = 1$.

The dipole moment functions for each normal mode are polynomial functions of the normal mode. These polynomial functions essentially form a Taylor expansion of the dipole moment function for each Cartesian component.

$$\mu_\rho(q) = \mu_\rho(q)_{q=0} + \frac{q}{1!}\left(\frac{\partial\mu_\rho(q)}{\partial q}\right)_{q=0} + \frac{q^2}{2!}\left(\frac{\partial^2\mu_\rho(q)}{\partial q^2}\right)_{q=0} + \cdots + \frac{q^n}{n!}\left(\frac{\partial^n\mu_\rho(q)}{\partial q^n}\right)_{q=0}$$

One of the restrictions of the double harmonic approximation is that this Taylor expansion is truncated at n=1. The transition dipole moment thereby becomes a summation of integrals of linear dipole moment functions for each Cartesian component, with i and j of 0 and 1, respectively.

$$|M_{ji}|^2 = \sum_\rho \left|\left\langle 0\left|\mu_\rho(q)_{q=0} + \frac{q}{1!}\left(\frac{\partial\mu_\rho(q)}{\partial q}\right)_{q=0}\right|1\right\rangle\right|^2$$

$$|M_{ji}|^2 = \left|\left\langle 0\left|\mu_x(q)_{q=0} + \frac{q}{1!}\left(\frac{\partial\mu_x(q)}{\partial q}\right)_{q=0}\right|1\right\rangle\right|^2 + \left|\left\langle 0\left|\mu_y(q)_{q=0} + \frac{q}{1!}\left(\frac{\partial\mu_y(q)}{\partial q}\right)_{q=0}\right|1\right\rangle\right|^2$$

$$+ \left|\left\langle 0\left|\mu_z(q)_{q=0} + \frac{q}{1!}\left(\frac{\partial\mu_z(q)}{\partial q}\right)_{q=0}\right|1\right\rangle\right|^2$$

2.3 Mass-weighted Hessian Matrix and Dimensionless Normal Mode Displacements

To find the harmonic frequencies of each normal mode, the Hessian matrix will need to be formed and diagonalized. The individual entries for the Hessian matrix will consist of second derivatives of the energies of the structure with respect to the Cartesian coordinates of one or two atoms. We estimated these derivatives as described below using a finite difference approach that required adjustments along the Cartesian coordinates of each atom, and attempted to conserve computational cost by considering adjustments along internal coordinates in place of Cartesian coordinates.

2.3.1 Cartesian Coordinates

The harmonic vibrational frequencies are found through diagonalization of a mass-weighted Hessian matrix. The Hessian matrix (D) is composed of second-order partial derivatives of the molecular potential energy surface with respect to one or two Cartesian coordinates of the atoms. For the HNO molecule, the Hessian matrix is a 9x9 square matrix. Laying the 2-dimensional HNO molecule along the xy-plane eliminates the translational motion along the z-axis and rotational motions of both the x-axis and y-axis. Considering only terms with x and y components reduces the matrix size to 6x6. The numbering 1-3 represent each of the three atoms in the HNO molecule.

$$D = \begin{bmatrix} \dfrac{\partial^2 U}{\partial x_1{}^2} & \dfrac{\partial^2 U}{\partial x_1 \partial y_1} & \dfrac{\partial^2 U}{\partial x_1 \partial x_2} & \dfrac{\partial^2 U}{\partial x_1 \partial y_2} & \cdots & \dfrac{\partial^2 U}{\partial x_1 \partial y_3} \\[2ex] \dfrac{\partial^2 U}{\partial y_1 \partial x_1} & \dfrac{\partial^2 U}{\partial y_1{}^2} & \dfrac{\partial^2 U}{\partial y_1 \partial x_2} & \dfrac{\partial^2 U}{\partial y_1 \partial y_2} & \cdots & \dfrac{\partial^2 U}{\partial y_1 \partial y_3} \\[2ex] \vdots & \vdots & \vdots & \vdots & \cdots & \vdots \\[2ex] \dfrac{\partial^2 U}{\partial y_3 \partial x_1} & \dfrac{\partial^2 U}{\partial y_3 \partial y_1} & \dfrac{\partial^2 U}{\partial y_3 \partial x_2} & \dfrac{\partial^2 U}{\partial y_3 \partial y_2} & \cdots & \dfrac{\partial^2 U}{\partial y_3{}^2} \end{bmatrix}$$

The Hessian matrix is converted into a mass-weighted Hessian matrix (D') with use of the diagonal mass-weighting matrix ($M^{1/2}$).

$$D' = M^{-1/2} D M^{-1/2}$$

Diagonalization of the mass-weighted matrix produces multiple eigenvalues (λ). Three of these eigenvalues are essentially zero, which come from the translational motion along the x-axis, the translational motion along the y-axis, and the rotational motion around the z-axis. The three non-zero eigenvalues represent the vibrational motion for each of the three normal modes. This follows the (3N-6) rule for number of vibrational modes in a non-linear molecule, such as HNO. These eigenvalues can be converted to vibrational frequency ($\hbar\omega$) by a direct relation to the eigenvalue.

$$\omega = \sqrt{\lambda}$$

Also produced by the diagonalization of D' are dimensionless normalized eigenvectors, one for each normal mode. These eigenvectors are converted to Cartesian displacement coordinates through a product of multiple matrices,

$$M^{-1/2} Q W^{-1}$$

Where Q is the matrix of the normalized eigenvectors, and W is the diagonal matrix of $\sqrt{\omega_i/\hbar}$.

The partial second derivatives of the Hessian matrix were approximated with the finite central difference method. For the diagonal Hessian entries, the coordinate of interest is adjusted from its optimized geometry by a small amount (h), which represents a "finite difference", in both the positive and negative directions and the energies for these new geometries are obtained and then inputted into the following formula to calculate the partial second derivative with respect to one coordinate.

$$\frac{\partial^2 U}{\partial x_1{}^2} = \frac{U(x_1 + h) - 2U(x_1) + U(x_1 - h)}{h^2}$$

For the off-diagonal Hessian entries, a similar approach is used but considering adjustments of two different coordinates by this finite difference.

$$\frac{\partial^2 U}{\partial x_1 \partial y_2} = \frac{U\begin{pmatrix} x_1 + h \\ y_2 + h \end{pmatrix} - U\begin{pmatrix} x_1 + h \\ y_2 - h \end{pmatrix} - U\begin{pmatrix} x_1 - h \\ y_2 + h \end{pmatrix} + U\begin{pmatrix} x_1 - h \\ y_2 - h \end{pmatrix}}{4h^2}$$

This central difference method is exact for a purely quadratic energy surface.

Although the 6x6 Hessian matrix contains 36 entries, the upper triangle of the matrix can be duplicated to make the lower triangle, which is a benefit of a symmetric matrix, such as the Hessian matrix when computing for the HNO molecule. This can be seen by noticing the finite difference formula is the same for $\frac{\partial^2 U}{\partial x_1 \partial y_2}$ as for $\frac{\partial^2 U}{\partial y_2 \partial x_1}$.

2.3.2 Internal Coordinates

The Hessian matrix entries of HNO consists of second derivatives of potential energy with respect to the 21 unique combinations of the six x- and y-Cartesian coordinates of individual atoms. To reduce computational cost, we computed the Hessian matrix with each entry consisting of second derivatives of potential energy with respect to the 6 combinations of the three internal coordinates. The three internal coordinates that describe the geometry of the HNO molecule are HN bond length, NO bond length, and the cosine of the bond angle. This essentially reduces our need of 72 *ab initio* calculations to 18 *ab initio* calculations for the Hessian matrix with this internal coordinate method.

2.4 Isotopic Effect

The quantitative displacement of each atom for a normal mode is described by the eigenvector of that normal mode. In experimental spectroscopy, when two vibrational frequencies are nearly equal to each other, it is possible that there will be strong coupling of the corresponding normal modes. Replacing one of the H, N, or O atoms with the next largest isotopes of ^{2}H, ^{15}N, or ^{18}O will shift certain vibrational frequencies and could decouple the normal modes that previously had nearby frequencies. ^{2}H substitution will have the largest effect in vibrational frequency shifts due to the large increase in reduced mass of the atoms involved in a vibration. Currently Anderson et al is experimenting with the ^{15}N isotope in HNO to determine the kinetic distinction between the ^{14}N and ^{15}N isotopomers. Performing isotopic substitution will

aid in Anderson's analysis of experimental spectroscopic data, as well as possibly confirm our vibrational normal mode assignments.

Each electronic energy is independent of the atomic masses of each atom. Therefore the isotopic effects yielding new harmonic frequencies, eigenvalues, and eigenvectors for selected isotopes can be studied without requiring new energetic calculations. Instead, the energetic calculations performed earlier for the Hessian matrix were used, and the only adjustment was altering the isotopic masses in creating the mass-weighted Hessian matrix (D') from the Hessian matrix.

2.5 Potential Energy Functions

The potential surface is important for the molar absorptivity calculations in providing the energy levels, the frequency, and force constants along each normal mode. The double harmonic approximation limits the potential energy as a function of each normal mode coordinate q to be a second-order function.

$$V(q) = V_{q=0} + constant * q^2$$

2.6 Dipole Moment Vectors

The other crucial component to calculating the molar absorptivity for each normal mode is the transition dipole moment which is comprised of dipole moment functions along each Cartesian direction. To find the dipole functions, the molecule was stretched and compressed along each normal mode. For each normal mode, the eigenvectors, once converted to Cartesian displacement coordinates, describe the amount of

displacement along each Cartesian coordinate that is attributed to the stretching or compression of that normal mode.

The molecule is initially at the optimized geometry. For each normal mode analysis, varying magnitudes of the normal mode are applied to the geometry by multiplying the unitless normal mode displacement with the eigenvector associated with a particular normal mode, and the initially optimized geometry is adjusted with this amount. *Ab initio* calculations at this new geometry provide the potential energy as well as dipole moment of this new configuration. This process is repeated along multiple amounts of the normal mode, including fractions of the normal mode. The resulting dipole moments are plotted against the normal mode.

With lower levels of theories in the *ab initio* calculations, such as MP2 and CCSD, a command can be directly inserted into the input file to retrieve the dipole moment of the new geometry in the output file. Higher levels of theory, like CCSD(T), however, require a different approach for the dipole moment. The new geometry must be placed in a uniform electric field oriented along the x- or y-axis, and these electric fields influence the potential energy of the molecule. The strength of the electric field is varied. The potential energy at each field strength is plotted against the strength of electric field (EF), and the negative first derivative of the potential energy with respect to the electric field at the field strength of zero gives the dipole moment vector of ρ, where $\rho = x \; or \; y$.

$$\overrightarrow{\mu_\rho} = -\left[\frac{\partial V}{\partial EF_\rho}\right]_{EF=0}$$

The dipole moments for a normal mode are then fit to a polynomial equation and the coefficient leading the linear term is proportional to the first derivative of the dipole moment with respect to the normal mode. This derivative is inserted into the double harmonic approximation of the transition dipole moment, which then, along with the harmonic frequency found previously from the Hessian matrix, gives the double harmonic molar absorptivity value for that specific normal mode. Anderson's experimental results are not directly comparable to our molar absorptivity values, but instead to a ratio of each pair of molar absorptivities. Hence, after having retrieved the theoretical molar absorptivity for each normal mode, such a ratio was created and compared to Anderson's results.

Chapter 3

Double Harmonic Results

3.1 Optimization and Harmonic Frequencies

The normal modes and vibrational frequencies of the HNO molecule were calculated through the double harmonic approximation and compared to those of T.J. Lee. However, Lee's data used a smaller basis set than the basis sets we considered (Lee 1993). The results that will be shown in this chapter and the next chapter will indicate that the double harmonic approximation breaks down for the HNO molecule.

The molecule was optimized using the aug-cc-pVTZ or aug-cc-pVQZ basis sets, with either the Hartree Fock, MP2, CCSD, or CCSD(T) levels of theory. The bond lengths and bond angle which yielded the minimal potential energy for each basis set and theory combination are detailed in Table 3.1.1. One clear pattern from the optimization results is that increasing the basis set with each theory results in a small change in the bond lengths and bond angle to yield the optimal energy. As basis set is increased, the decrease in optimal energy from Hartree-Fock to the electron-electron correlation considering methods (MP2, CCSD, CCSD(T)) is greater than the differences in energy between the electron correlation methods, which demonstrates the importance of including electron correlation in the *ab initio* calculations. Within each basis set, the minimal energy decreases when considering Hartree Fock to MP2 to CCSD to CCSD(T), thus showing consistency across the theories.

After obtaining the optimal bond lengths and bond angle and placing the atoms on a xy-plane, as described in Chapter 2, the x- and y- coordinates of each atom were displaced by a small value of h = 0.01 Å. As expected, each adjustment of a coordinate resulted in a new and higher energy than the energy for the optimized geometry. The

Table 3.1.1. HNO optimization results for each basis set and theory. Optimal parameters listed are NH bond length (Å), NO bond length (Å), bond angle (in degrees), and optimal energy (Hartrees).

Basis Set	Theory	R_{NH} (Å)	R_{NO} (Å)	bond angle (°)	Energy (Ha)
aug-cc-pVTZ	HF	1.03034	1.16610	109.38	-129.84295114
	MP2	1.05068	1.22167	107.65	-130.28424878
	CCSD	1.05173	1.20371	108.25	-130.28878822
	CCSD(T)	1.05527	1.21518	107.98	-130.30975046
aug-cc-pVQZ	HF	1.02986	1.16468	109.40	-129.85158882
	MP2	1.04924	1.21773	107.77	-130.31997667
	CCSD	1.04979	1.19972	108.35	-130.32035738
	CCSD(T)	1.05331	1.21104	108.10	-130.34262935

central difference method used these energies to formulate an approximation for the second derivatives of the potential energy of HNO with respect to the x- and y-coordinates of each atom. The diagonalization of the 6 x 6 Hessian matrix yielded six eigenvalues, three of which were zero, specifically for the x-translational mode, y-translational mode, and the z-rotational mode. The three non-zero eigenvalues were for the three vibrational modes, which is consistent with the (3N-6) rule. The vibrational eigenvalues were converted to the three harmonic vibrational frequencies. Table 3.1.2 shows the harmonic frequencies obtained from each basis set and computational theory. The first labeled frequency, ω_1, is the highest in wavenumbers and the third labeled frequency, ω_3, is the lowest, and this notation will be consistent throughout this document.

Just as with the results of optimization, Table 3.1.2 shows that for the vibrational frequencies there is more disagreement between levels of theory than between basis sets. For both basis sets, as theory increases from Hartree Fock, which does not take into account the electron-electron correlation, to MP2, all of the vibrations display a distinctly large decrease of several hundred wavenumbers in harmonic frequency. This large decrease in frequency from Hartree-Fock to MP2 resulted in more agreement to experimental frequencies (Ruzi and Anderson 2015). This demonstrates the importance of including electron correlation to correctly describe each vibrational behavior.

ω_2 and ω_3 exhibit an increase of just below 100 cm^{-1} as the theory changes from MP2 to CCSD. The CCSD(T) frequency values for ω_2 and ω_3 are between the MP2 and CCSD values. Similar to the lower vibrational frequencies, ω_1 shows a decrease as

26

Table 3.1.2. Harmonic frequency (cm^{-1}) results for each normal mode using each basis set and theory. These results are from Hessian entries of second derivatives with respect to Cartesian coordinates of the atoms.

Basis Set	Theory	ω_1	ω_2	ω_3
aug-cc-pVTZ	HF	3307.3	1934.9	1706.2
	MP2	3031.1	1577.7	1475.8
	CCSD	3003.6	1662.0	1582.7
	CCSD(T)	2950.4	1593.4	1535.7
aug-cc-pVQZ	HF	3307.1	1939.0	1708.3
	MP2	3037.9	1583.8	1490.2
	CCSD	3018.7	1677.4	1586.8
	CCSD(T)	2964.6	1602.1	1544.2

theory is adjusted from MP2 to CCSD, but with a smaller shift in wavenumbers of less than 30 cm^{-1}. Unlike with ω_2 and ω_3, the frequency of ω_1 continues to decrease when coupled-cluster theory considers a perturbative treatment of triple excitations.

The eigenvectors that were calculated for each mode from the diagonalization of the mass-weighted Hessian matrix described the displacement of each atom along the x- and y-directions. To get a general depiction of which vibration was described by which normal mode, multiples of each normal mode were applied by positive and negative magnitudes and the resulting changes in the NH bond length, NO bond length, and the HNO bond angle were noticed. The q1 mode almost entirely described the NH bond length. The q2 and q3 modes, however, had a great influence on both the NO bond length and the HNO bond angle.

3.2 Isotope Substitution Effect

The vibrational frequencies with isotopic substitution of ^{15}N with differing basis sets and theories are listed in Table 3.2.1. All three vibrational modes were expected to be affected by the ^{15}N substitution, as nitrogen is the central atom of the triatomic molecule and has contribution to the NH stretch, NO stretch, and HNO bend. As expected, Table 3.2.1 shows this trend. Although ω_1 experiences an almost constant decrease with the ^{15}N substitution, the other modes experience an inconsistent shift depending on computational theory applied. At times ω_2 experiences a larger decrease while ω_3 experiences a lower decrease, and at other times ω_2 experiences a lower decrease while ω_3 experiences a larger decrease. Due to this inconsistent behavior of

Table 3.2.1. Harmonic frequency (cm^{-1}) results for each normal mode using each basis set and theory for the HNO molecule with the ^{15}N isotopic substitution. These results are from Hessian entries of second derivatives with respect to Cartesian coordinates of the atoms. Values in parenthesis are the frequency shifts from the ^{1}H^{14}N^{16}O molecule using the same basis set and theory.

Basis Set	Theory	ω_1	ω_2	ω_3
aug-cc-pVTZ	HF	3300.2 (-7.1)	1901.2 (-33.7)	1700.2 (-6.0)
	MP2	3024.3 (-6.8)	1572.7 (-5.1)	1450.0 (-25.8)
	CCSD	2997.0 (-6.6)	1640.2 (-21.8)	1570.5 (-12.1)
	CCSD(T)	2943.9 (-6.5)	1584.4 (-9.0)	1512.5 (-23.1)
aug-cc-pVQZ	HF	3300.0 (-7.1)	1905.2 (-33.8)	1702.3 (-6.0)
	MP2	3031.1 (-6.8)	1578.2 (-5.6)	1464.6 (-25.6)
	CCSD	3012.1 (-6.5)	1653.7 (-23.8)	1576.3 (-10.6)
	CCSD(T)	2958.1 (-6.5)	1589.9 (-12.2)	1523.8 (-20.3)

these shifts in frequency between ω_2 and ω_3, it is may be beneficial to include a higher level theory until consistency is found. After including a full treatment of triple excitations, as in CCSDT, if frequencies are found to agree between CCSD(T) and CCSDT, this can assure us that CCSD(T) level of theory is sufficient.

The vibrational frequencies with isotopic substitution of [18]O are listed in Table 3.2.2. As stated previously, the NH stretch was most largely attributed to arise from the q1 mode, while q2 and q3 were both found to a great contribution to both the NO stretch and the HNO bend. As the NO stretch and HNO bend both involve oxygen directly, the [18]O substitution was predicted to have the greatest influence on the q2 and q3 modes. This expected behavior is shown in Table 3.2.2, however the magnitude of shifts are inconsistent, as was noted earlier with the nitrogen substitution.

The resulting frequencies from the ^{2}H substitution in the HNO molecule are shown in Table 3.2.3. Hydrogen is major component in both the HN stretch and the HNO bend. Since the HN stretch is most affected by the q1 mode, the vibrational frequency of the q1 mode is expected to be largely altered by the ^{2}H substitution. The HNO bend, however, was shown to be largely affected by both the q2 and q3 modes. As seen in Table 3.2.3, the highest frequency is now nearly 800 cm^{-1} lower than highest frequency of the non-isotopically substituted molecule, and the lowest frequency is now nearly 300-400 cm^{-1} lower than the lowest frequency of the non-isotopically substituted molecule. It is not clear which of the q2 and q3 modes from the non-isotopically substituted molecule resulted in the lowest frequency with the ^{2}H substitution. If identification of the modes is an interest in the future, the HNO molecule should be

Table 3.2.2. Harmonic frequency (cm^{-1}) results for each normal mode using each basis set and theory for the HNO molecule with the ^{18}O isotopic substitution. These results are from Hessian entries of second derivatives with respect to Cartesian coordinates of the atoms. Values in parenthesis are the frequency shifts from the ^{1}H^{14}N^{16}O molecule using the same basis set and theory.

Basis Set	Theory	ω_1	ω_2	ω_3
aug-cc-pVTZ	HF	3307.1 (-0.2)	1883.2 (-51.7)	1701.4 (-4.8)
	MP2	3030.9 (-0.2)	1563.2 (-14.5)	1445.7 (-30.0)
	CCSD	3003.3 (-0.3)	1619.0 (-43)	1577.0 (-5.6)
	CCSD(T)	2950.1 (-0.3)	1571.5 (-21.9)	1511.5 (-24.2)
aug-cc-pVQZ	HF	3306.9 (-0.2)	1887.2 (-51.8)	1703.4 (-4.8)
	MP2	3037.7 (-0.2)	1568.0 (-15.8)	1461.0 (-29.2)
	CCSD	3018.4 (-0.3)	1632.6 (-44.8)	1582.5 (-4.4)
	CCSD(T)	2964.3 (-0.3)	1574.1 (-28)	1525.5 (-18.7)

Table 3.2.3. Harmonic frequency (cm^{-1}) results for each normal mode using each basis set and theory for the HNO molecule with the ^{2}H isotopic substitution. These results are from Hessian entries of second derivatives with respect to Cartesian coordinates of the atoms. Values in parenthesis are the frequency shifts from the ^{1}H^{14}N^{16}O molecule using the same basis set and theory.

Basis Set	Theory	ω_1	ω_2	ω_3
aug-cc-pVTZ	HF	2416.8 (-890.5)	1934.2 (-0.7)	1289.9 (-416.2)
	MP2	2217.4 (-813.7)	1498.4 (-79.4)	1169.7 (-306.1)
	CCSD	2196.4 (-807.2)	1653.5 (-8.5)	1198.7 (-394.0)
	CCSD(T)	2158.1 (-792.3)	1563.1 (-30.3)	1178.4 (-357.3)
aug-cc-pVQZ	HF	2416.6 (-890.5)	1938.3 (-0.6)	1291.6 (-416.7)
	MP2	2222.3 (-815.6)	1514.4 (-69.4)	1173.4 (-316.8)
	CCSD	2207.1 (-811.6)	1670.7 (-6.8)	1201.4 (-385.4)
	CCSD(T)	2168.4 (-796.3)	1580.3 (-21.8)	1179.4 (-364.8)

studied with several small incremental hydrogen mass changes until reaching the ^{2}H mass. Then, the observation of the smaller frequency shifts with each mass adjustment will help understand the frequency behavior each mode experiences.

3.3 Internal Coordinates

Changing the entries of the Hessian matrix from second derivatives of the potential energy with respect to two Cartesian coordinates to matrix entries expressed in terms of derivatives with respect to the internal coordinates reduces the computational time substantially, as there are far more deviations to consider when considering the six Cartesian coordinates than when considering only three internal coordinates. The three internal coordinates were the NH bond length, NO bond length, and cosine of the molecular angle. Table 3.3.1 lists the frequencies of the HNO molecule and the frequencies of the molecule's isotopic substitutions. The largest disagreement from the Hessian resultant frequencies calculated using internal coordinates compared to using Cartesian coordinates is less than 3.0 cm^{-1}. This indicates a good agreement of frequencies between internal and Cartesian coordinates, as much larger differences in frequencies were noticed earlier when studying the effect of basis sets and computational theories with Cartesian coordinates alone. The agreement of frequencies from using internal coordinates compared to using Cartesian coordinates for the Hessian calculation, along with the benefit of four times reduction of computational cost, motivates us to consider future work with the Hessian matrix to be from computations of geometries adjusted along internal coordinates in place of Cartesian coordinates.

Table 3.3.1. Harmonic frequency (cm^{-1}) results for each normal mode considering internal coordinates, using aug-cc-pVQZ and CCSD(T) for the HNO molecule without isotopic substitution, and for the molecule with the ^{2}H isotopic substitution, with the ^{15}N isotopic substitution, and with the ^{18}O isotopic substitution. These results are from Hessian entries of second derivatives with respect to internal coordinates of the atoms. Values in parenthesis are the frequency shifts from the same isotopes using aug-cc-pVQZ and CCSD(T) with considering Cartesian coordinates.

	ω_1	ω_2	ω_3
^{1}H^{14}N^{16}O	2963.0 (-1.6)	1600.2 (-1.9)	1542.2 (-2.0)
^{2}H^{14}N^{16}O	2167.4 (-1.0)	1579.7 (-0.6)	1176.7 (-2.7)
^{1}H^{15}N^{16}O	2956.5 (-1.6)	1587.6 (-2.3)	1522.4 (-1.4)
^{1}H^{14}N^{18}O	2962.8 (-1.6)	1571.2 (-2.9)	1524.5 (-1.0)

3.4 Double Harmonic Potential Energy Functions

It is assumed in the double harmonic approximation that potential energies that are functions of normal modes can be sufficiently described by a quadratic function. The coefficient leading the normal mode is the harmonic force constant. Manipulation of the harmonic frequency that was retrieved from diagonalization of the Hessian matrix yields the harmonic force constant. The optimal energy and force constant of each normal mode would create the quadratic potential energy function of each normal mode.

Figures 3.4.1, 3.4.2, and 3.4.3 show data points for *ab initio* potential energies resulting from the geometrical changes from the HNO optimal geometry by normal modes 1, 2, and 3, respectively. As described above, to model the double harmonic potential energy certain parameters are already set, specifically the optimal energy and the harmonic force constant. For each figure, the line in red is a best fit sixth-power polynomial function that best describes the trend set by the collection of the individual potential energies. To see the quantitative influence of the higher polynomials in describing the trend of the collective potential energies, the sixth-power potential energy expression is given in each figure.

Figure 3.4.1 shows the potential energy behavior for the q1 mode, and this mode, as described earlier, predominately describes the HN bond vibration. By visual inspection alone it can be seen that the behavior of the energies would not be explained well by a symmetric quadratic function. This indicates that the next several orders beyond the second order are important to accurately describe the potential energy function.

Energy vs. q1

$$V(q) = -130.3426293322 + 6.7503 \cdot 10^{-3}\, q^2 - 1.5910 \cdot 10^{-3}\, q^3$$
$$+ 2.5944 \cdot 10^{-4}\, q^4 - 5.9866 \cdot 10^{-5}\, q^5 + 6.8307 \cdot 10^{-6}\, q^6$$
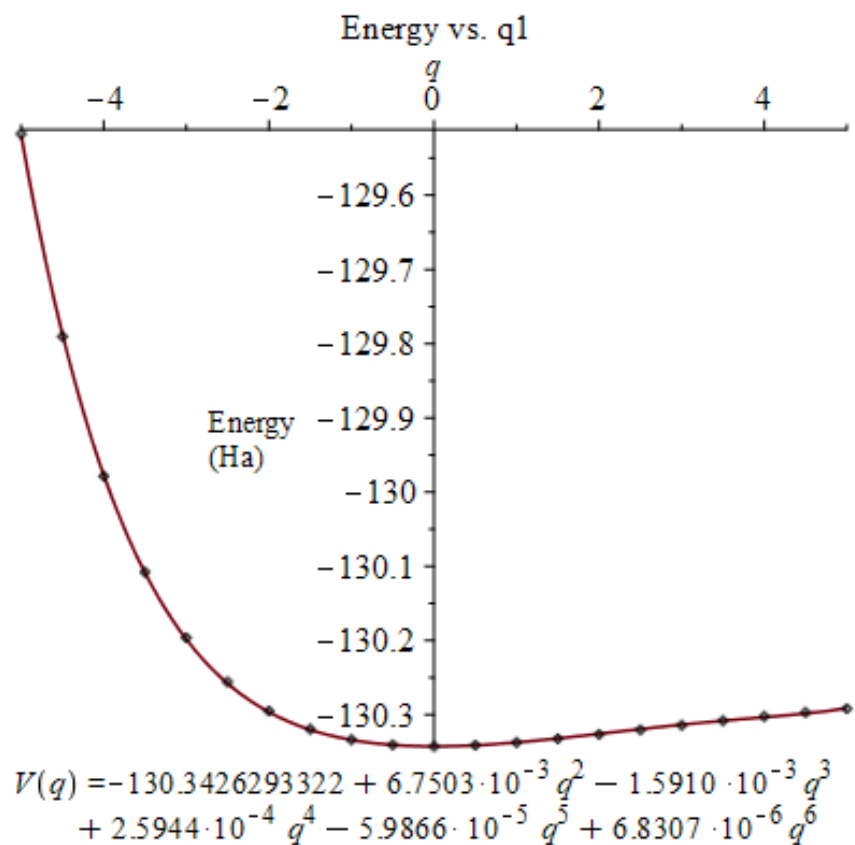
Figure 3.4.1. Aug-cc-pVQZ, CCSD(T) *ab initio* **potential energies vs. q1 mode for the q1 mode resultant from internal coordinate Hessian matrix.** The sixth order polynomial fit is an expansion to the double harmonic potential energy function.
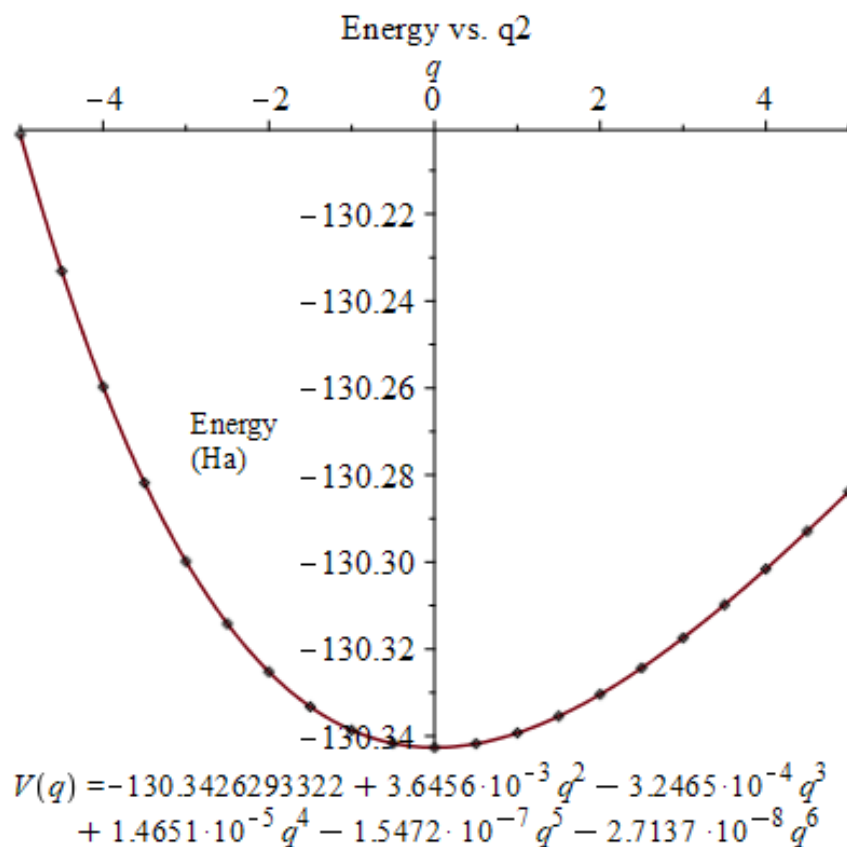
Figure 3.4.2. Aug-cc-pVQZ, CCSD(T) *ab initio* potential energies vs. q2 mode for the q2 mode resultant from internal coordinate Hessian matrix. The sixth order polynomial fit is an expansion to the double harmonic potential energy function.

Energy vs. q3

$$V(q) = -130.3426293322 + 3.5133 \cdot 10^{-3} q^2 + 1.0722 \cdot 10^{-4} q^3$$
$$+ 4.0898 \cdot 10^{-6} q^4 - 8.6099 \cdot 10^{-7} q^5 - 3.5053 \cdot 10^{-7} q^6$$
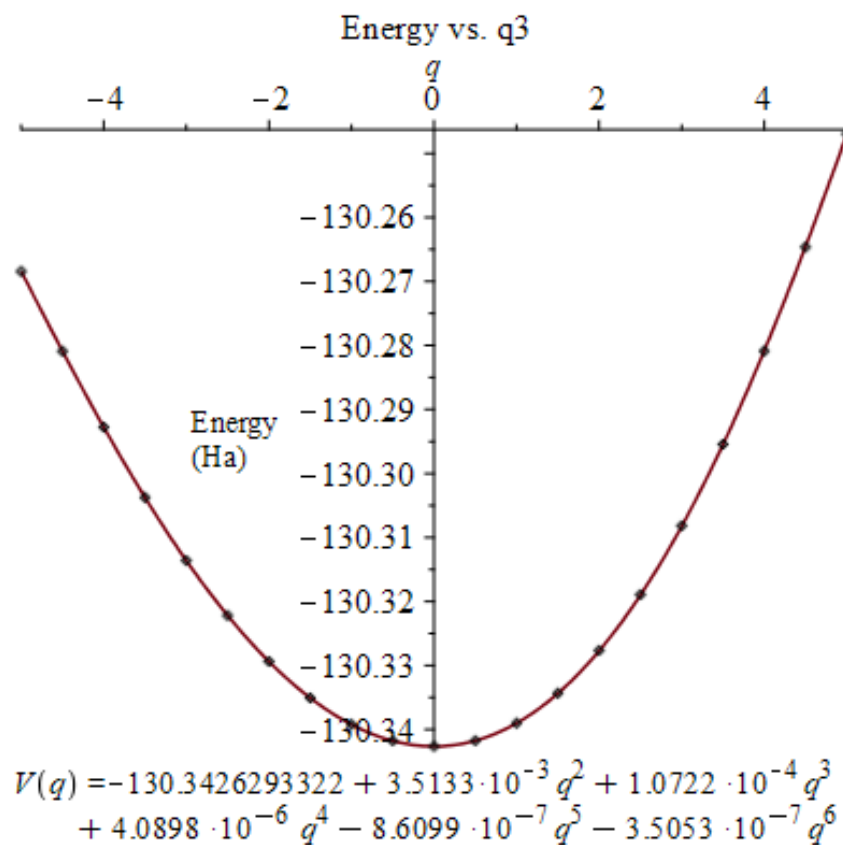
Figure 3.4.3. Aug-cc-pVQZ, CCSD(T) *ab initio* **potential energies vs. q3 mode for the q3 mode resultant from internal coordinate Hessian matrix.** The sixth order polynomial fit is an expansion to the double harmonic potential energy function.

The quantitative contributions of higher orders are not as significant in the potential energy functions which describe the q2 and q3 modes, given in Figures 3.4.2 and 3.4.3, respectively. However it is apparent from a visual inspection of both of the potential energy behaviors relative to their normal modes that terms beyond the second order are necessary to correctly describe the functions.

3.5 Double Harmonic Dipole Moment Functions

The transition dipole moment is made up x- and y-components of the dipole moment functions of normal modes. The double harmonic approximation assumes a linear function to adequately describe the behavior of these dipole moments.

The x-component of the dipole moments with geometrical changes of q1, q2, and q3 modes are displayed in Figures 3.5.1, 3.5.2, and 3.5.3, respectively. The red line is a fifth-power function best fit to the *ab initio* data of the x-component dipole moments. It is both visually and quantitatively clear that the x-component dipole moments for the q1 and q3 modes, especially, have a great contribution from the higher powers.

The y-component of the dipole moments with geometrical changes of q1, q2, and q3 modes, displayed in Figures 3.5.4, 3.5.5, and 3.5.6, respectively, give a similar trend as that described for the x-component dipole moment, except the y-component dipole moment for q2 shows an especially stronger non-linear behavior than for the x-component dipole moment for q2.

x-component of Dipole Moment vs. q1

$$\mu_x(q) = -0.357725 + 0.0380130\, q + 0.00996687\, q^2$$
$$- 0.000295982\, q^3 - 0.000109344\, q^4 - 3.09509\ 10^{-6}\, q^5$$
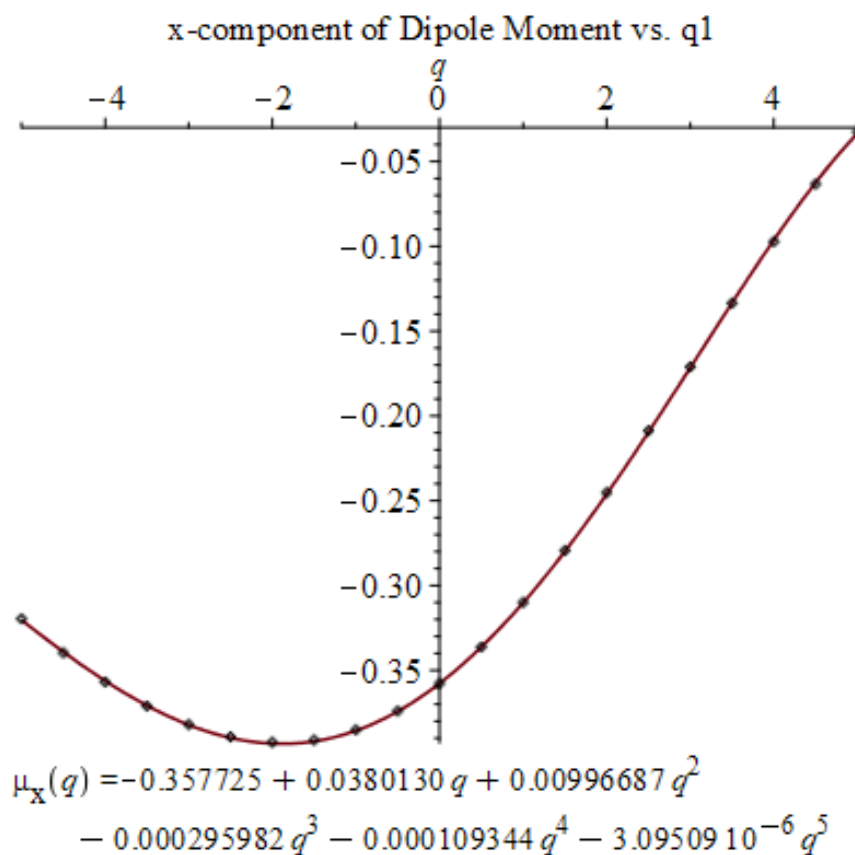
Figure 3.5.1. Aug-cc-pVQZ, CCSD(T) *ab initio* **x-component of dipole moment vs. q1 mode for the q1 mode resultant from internal coordinate Hessian matrix.** The fifth order polynomial fit is an expansion to the double harmonic dipole moment function.

x-component of Dipole Moment vs. q2

$$\mu_x(q) = -0.357725 - 0.0636210\,q + 0.00342970\,q^2$$
$$- 0.000221774\,q^3 + 0.0000128940\,q^4 - 9.9130\cdot 10^{-7}q^5$$
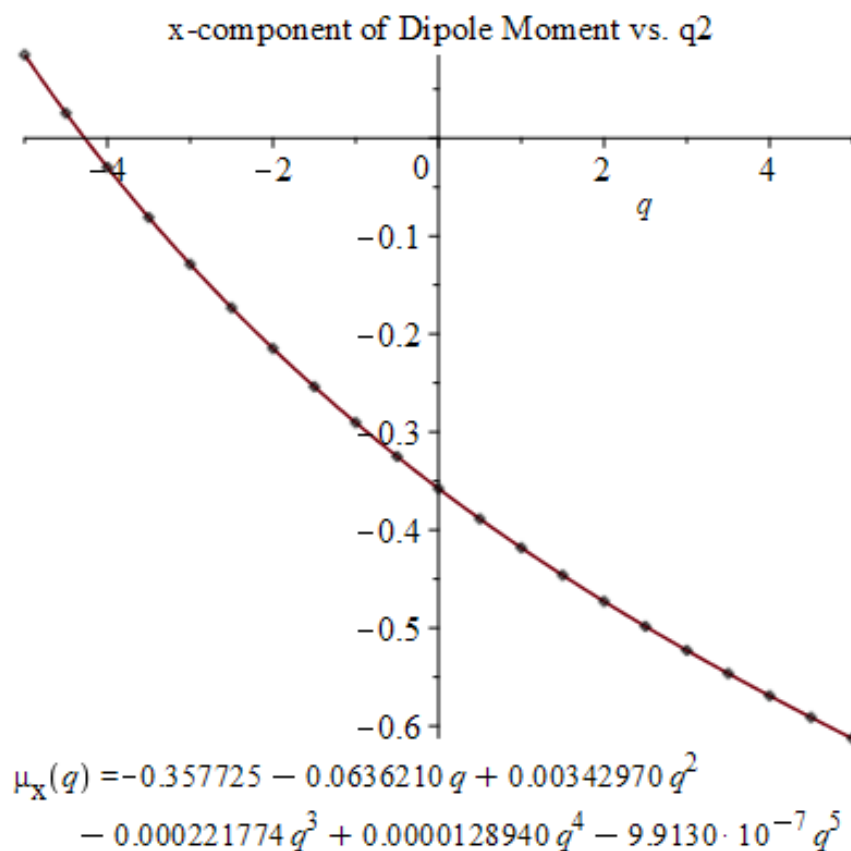
Figure 3.5.2. Aug-cc-pVQZ, CCSD(T) *ab initio* **x-component of dipole moment vs. q2 mode for the q2 mode resultant from internal coordinate Hessian matrix.** The fifth order polynomial fit is an expansion to the double harmonic dipole moment function.

x-component of Dipole Moment vs. q3

$$\mu_x(q) = -0.357725 - 0.00549511\,q + 0.00654864\,q^2$$
$$+ 0.00106551\,q^3 + 0.000152683\,q^4 + 6.36951 \cdot 10^{-6}\,q^5$$
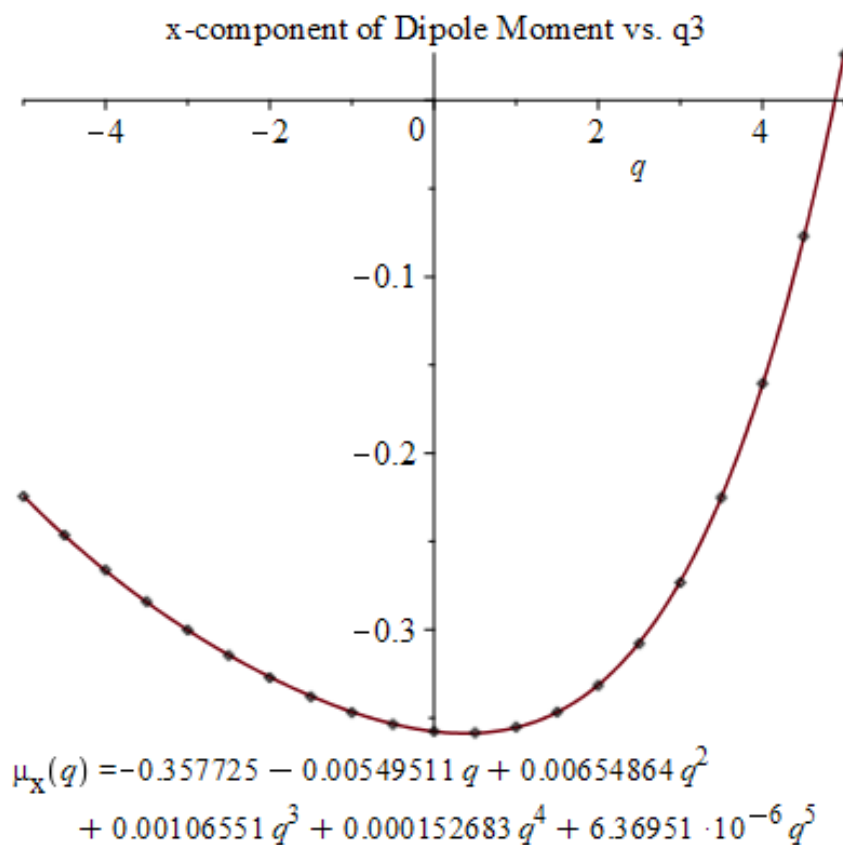
Figure 3.5.3. Aug-cc-pVQZ, CCSD(T) *ab initio* **x-component of dipole moment vs. q3 mode for the q3 mode resultant from internal coordinate Hessian matrix.** The fifth order polynomial fit is an expansion to the double harmonic dipole moment function.

y-component of Dipole Moment vs. q1

$$\mu_y(q) = 0.560625 - 0.0550488\,q - 0.0140932\,q^2$$
$$+ 0.000313411\,q^3 + 0.000171847\,q^4 + 9.27933 \cdot 10^{-6}\,q^5$$
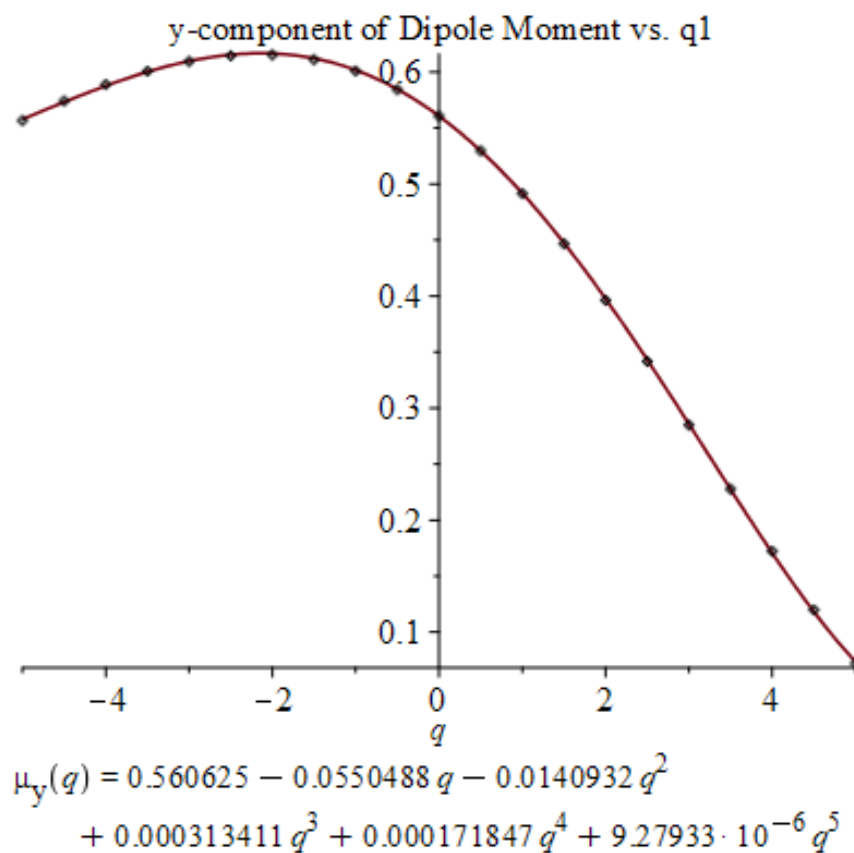
Figure 3.5.4. Aug-cc-pVQZ, CCSD(T) *ab initio* **y-component of dipole moment vs. q1 mode for the q1 mode resultant from internal coordinate Hessian matrix.** The fifth order polynomial fit is an expansion to the double harmonic dipole moment function.

y-component of Dipole Moment vs. q2

$$\mu_y(q) = 0.560625 + 0.0235823\,q - 0.00428905\,q^2$$
$$+\ 0.000306325\,q^3 - 0.0000585216\,q^4 + 6.0120 \cdot 10^{-6}\,q^5$$
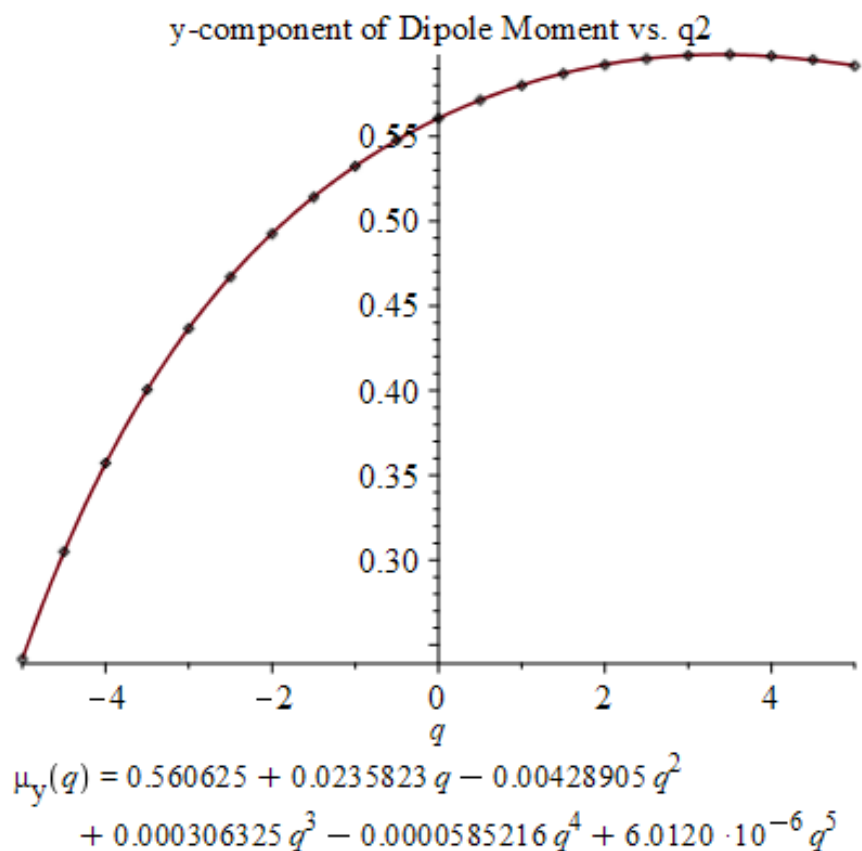
Figure 3.5.5. Aug-cc-pVQZ, CCSD(T) *ab initio* **y-component of dipole moment vs. q2 mode for the q2 mode resultant from internal coordinate Hessian matrix.** The fifth order polynomial fit is an expansion to the double harmonic dipole moment function.

y-component of Dipole Moment vs. q3

$$\mu_y(q) = 0.560625 - 0.0177716\,q - 0.00944899\,q^2$$
$$- 0.00127817\,q^3 - 0.0000273135\,q^4 + 5.73148 \cdot 10^{-6}\,q^5$$
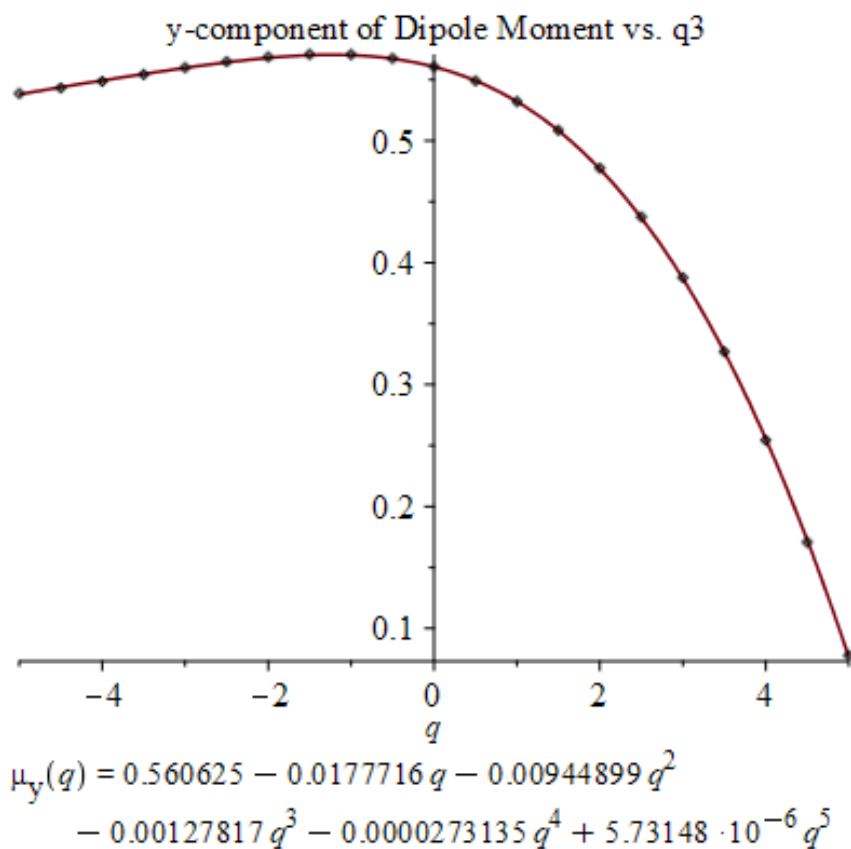
Figure 3.5.6. Aug-cc-pVQZ, CCSD(T) *ab initio* **y-component of dipole moment vs. q3 mode for the q3 mode resultant from internal coordinate Hessian matrix.** The fifth order polynomial fit is an expansion to the double harmonic dipole moment function.

Chapter 4

Anharmonicity and Coupling

4.1 Introduction

The potential energy and dipole moment behaviors of each normal mode were graphically shown in Chapter 3 to not be described sufficiently well by the double harmonic approximation. This chapter explores expanding the potential energy function beyond a quadratic function and the dipole moment function beyond a linear function, and including these expanded functions in the determination of the transition dipole moment. The inclusion of these expanded functions is known as considering effects of both mechanical and electrical anharmonicity. Mechanical anharmonicity is the potential energy anharmonicity, and electrical anharmonicity is the dipole moment anharmonicity. This chapter will also look into coupling of normal modes.

4.1.1 Complete Potential Energy

The true potential energy of the HNO molecule is a system of contributions from all three vibrational normal modes. The double harmonic approximation has a very simple potential energy equation. Below, V_{opt} represents the minimal energy found at the optimal geometry, where q1 = q2 = q3 = 0.

$$V_{DHA}(q_1 q_2 q_3) = V_{opt} + \frac{\hbar\omega_1}{2}q_1{}^2 + \frac{\hbar\omega_2}{2}q_2{}^2 + \frac{\hbar\omega_3}{2}q_3{}^2$$

The harmonic frequencies were found from diagonalizing the Hessian matrix. The computational cost to formulate this equation is near equivalent to the sum of the cost of individual *ab initio* calculations required to formulate the Hessian matrix. As mentioned earlier, computing the Hessian matrix with internal coordinates reduces the computational cost by 75% when compared to Cartesian coordinates. The Cartesian

coordinates require 72 *ab initio* calculations, whereas using internal coordinates requires only 18 *ab initio* calculations.

The full potential energy, however, is composed of terms higher than quadratic for each individual mode. Including mechanical anharmonic contributions from each normal mode extends the potential energy equation to include individual mode contributions beyond the second power.

$$V_{DHA+ANHARM}(q_1 q_2 q_3) = V_{DHA}(q_1 q_2 q_3) + k_{111}q_1^3 + k_{222}q_2^3 + k_{333}q_3^3 + k_{1111}q_1^4 + \cdots$$

Here, the coefficients leading the individual normal modes represent the powers to which the normal mode was applied. For example, k_{111} represents the coefficient leading the q_1 mode to the third power.

The full potential energy equation also includes an additional important concept that is ignored in the double harmonic approximation, which is the coupling between normal modes. The mechanical coupling of two or more modes will affect the potential energy of the molecule, with differing effects that depend on the modes that are coupled. Generally, modes are more likely to couple the closer the vibrational frequencies of the modes are to one another.

$$V_{DHA+ANHARM+COUPLING}(q_1 q_2 q_3)$$
$$= V_{DHA+ANHARM}(q_1 q_2 q_3) + k_{112}q_1^2 q_2 + k_{122}q_1 q_2^2 + k_{113}q_1^2 q_3 + k_{133}q_1 q_3^2$$
$$+ k_{223}q_2^2 q_3 + k_{233}q_2 q_3^2 + k_{1122}q_1^2 q_2^2 + \cdots$$

4.1.2 Complete Dipole Moment

The dipole function for each Cartesian component, ρ, assumed by the double harmonic approximation is limited to a first power.

$$\mu_{DHA,\rho}(q_1 q_2 q_3) = \mu_{opt} + c_1 q_1 + c_2 q_2 + c_3 q_3$$

Moving beyond this approximation and including electrical anharmonicity leads to the individual normal modes contributing higher powers to the dipole function.

$$\mu_{DHA+ANHARM,\rho}(q_1 q_2 q_3) = \mu_{DHA,\rho}(q_1 q_2 q_3) + c_{11}q_1{}^2 + c_{22}q_2{}^2 + c_{33}q_3{}^2 + c_{111}q_1{}^3 + \cdots$$

And finally, including electrical coupling between the normal modes gives the full dipole function for each Cartesian component, ρ.

$$\mu_{DHA+ANHARM+COUPLING,\rho}(q_1 q_2 q_3)$$

$$= \mu_{DHA+ANHARM,\rho}(q_1 q_2 q_3) + c_{12}q_1 q_2 + c_{13}q_1 q_3 + c_{23}q_2 q_3 + c_{112}q_1{}^2 q_2 + \cdots$$

4.2 Anharmonicity

The anharmonic wavefunction (ψ_{anharm}) for each vibrational level consists of a linear combination of harmonic oscillator wavefunctions (ϕ_{harm}) at vibrational states *v=0* through *v=n*. Due to Anderson's kinetic infrared studies specializing specifically in the i = 0 to j = 1 transitions, we only considered the anharmonic wavefunctions for the v=0 and v=1 vibrational states.

$$\psi_{anharm,v=0}(q) = b_0 \phi_{harm,v=0}(q) + b_1 \phi_{harm,v=1}(q) + \cdots + b_n \phi_{harm,v=n}(q)$$

$$\psi_{anharm,v=1}(q) = c_0 \phi_{harm,v=0}(q) + c_1 \phi_{harm,v=1}(q) + \cdots + c_n \phi_{harm,v=n}(q)$$

The b coefficients represent the contributions of each harmonic oscillator vibrational level function needed for defining the anharmonic wavefunction at v=0, and the c coefficients represent the same but for defining the anharmonic wavefunction at v=1. The sum of the coefficients squared is equal to one, and the value of each coefficient squared represents the weighted contribution from each harmonic wavefunction towards the anharmonic wavefunction.

For the following anharmonic work, we used expanded potential energy functions to the sixth power. Lower polynomial expansions were also tested but each next higher expansion resulted in a more accurate fit to the *ab initio* results. The sixth order functions' mean absolute deviation values were 9.8×10^{-4} Ha for q1, 9.0×10^{-6} Ha for q2, and 2.7×10^{-5} Ha for q3. As with the harmonic potential energy functions in Chapters 2 and 3, the optimal energy and Hessian-derived harmonic frequency converted to the second order force constant were used to make up the harmonic portion of the potential energy function of each mode. The expanded dipole moment functions we used were to the fifth power. As mentioned previously, we considered harmonic wavefunctions of the ground vibrational state and up to and including the third harmonic vibrational state.

4.2.1 Electrical Anharmonicity

We first considered contributions from electrical anharmonicity alone. Since mechanical anharmonicity was not yet considered, only the harmonic wavefunction at the vibrational state of the anharmonic wavefunction will contribute to the anharmonic wavefunction. That is for $\psi_{anharm,v=0}(q)$, only $\phi_{harm,v=0}(q)$ will contribute, and similarly for $\psi_{anharm,v=1}(q)$, only $\phi_{harm,v=1}(q)$ will contribute. Therefore b_0 and c_1 will have full

weight on the $\psi_{anharm,v=0}(q)$ and $\psi_{anharm,v=1}(q)$ anharmonic wavefunctions, respectively. Since the potential is still harmonic, a harmonic Hamiltonian is computed.

With considering electrical anharmonicity, the dipole moment function can be treated as a Taylor expansion.

$$\mu_\rho(q) = \mu_\rho(q)_{q=0} + \frac{q}{1!}\left(\frac{\partial \mu_\rho(q)}{\partial q}\right)_{q=0} + \frac{q^2}{2!}\left(\frac{\partial^2 \mu_\rho(q)}{\partial q^2}\right)_{q=0} + \cdots + \frac{q^n}{n!}\left(\frac{\partial^n \mu_\rho(q)}{\partial q^n}\right)_{q=0}$$

Now the transition dipole moment becomes more intricate than earlier with the double harmonic approximation. Assuming that we allow both the x and y dipole moment functions to include up to nth order contributions, and considering harmonic contributions up to the vibrational state of 3, the transition moment squared becomes the following.

$$|M_{ji}|^2 = \sum_\rho \left| \sum_{i=0}^{3}\sum_{j=0}^{3} b_i * c_j * \left[(\mu_\rho)_{q=0}\langle i|j\rangle + \frac{\left(\frac{\partial \mu_\rho}{\partial q}\right)_{q=0}}{1!}\langle i|q|j\rangle + \cdots + \frac{\left(\frac{\partial^n \mu_\rho}{\partial q^n}\right)_{q=0}}{n!}\langle i|q^n|j\rangle \right] \right|^2$$

The integrals up to $\langle i|q^n|j\rangle$ were simplified by defining the q operator using ladder operators. Using raising and lowering operators resulted in each integral becoming a constant multiplied by a much simpler integral of the form $\langle i|m\rangle$ where m represented some additive of j.

$$|M_{ji}|^2 = \sum_\rho \left| \sum_{i=0}^{3} \sum_{j=0}^{3} b_i * c_j \right.$$

$$* \left[(\mu_\rho)_{q=0} \langle i|j \rangle + \frac{\left(\frac{\partial \mu_\rho}{\partial q}\right)_{q=0}}{1!} * const\langle i|m \rangle + \cdots + \frac{\left(\frac{\partial^n \mu_\rho}{\partial q^n}\right)_{q=0}}{n!} * const'\langle i|m' \rangle \left. \right] \right|^2$$

Since these harmonic wavefunctions are orthonormal to each other, the integrals result in a value of 1 or 0 using Kronecker delta. The molar absorptivities of each normal mode were calculated using this transition dipole moment, along with the harmonic frequency.

4.2.2 Electrical and Mechanical Anharmonicity

Next we included both electrical and mechanical anharmonicity. The combinations of the harmonic components of the Hamiltonian matrix with the anharmonic components gave us the anharmonic vibrational state eigenvalues and the corresponding eigenvector. The eigenvector corresponding to the lowest energy eigenvalue gave us the contribution of each harmonic wavefunction for the ground state v=0 anharmonic wavefunction. Similarly, the eigenvector corresponding to the second lowest eigenvalue gave us the contribution of each harmonic wavefunction for the v=1 anharmonic wavefunction. As described earlier, the linear combination of these coefficients multiplied by the corresponding harmonic wavefunction gave us the anharmonic wavefunction for the particular vibrational level.

Table 4.2.1 lists the resultant b and c eigenvectors for each normal mode when considering contributions from the ground vibrational state (v=0) up to and including the third excited vibrational state of v=3. As seen for each mode, the anharmonic wavefunction for the ground vibrational state has the largest coefficient coming from the v=0 harmonic vibrational state, which indicates the v=0 harmonic wavefunction has the most contribution to the ground state anharmonic wavefunction. There is a considerable contribution from each of the excited harmonic wavefunctions as well, with the largest of these from the v=1 harmonic wavefunction. The highest contribution from the v=1 harmonic wavefunction towards the anharmonic ground state wavefunction comes from the q1 mode.

The anharmonic wavefunction for the first excited vibrational state is mostly made up of the v=1 vibrational state harmonic wavefunction. The largest contribution from other harmonic wavefunctions comes from the q1 mode. The largest anharmonic effects for both v=0 and v=1 anharmonic wavefunctions come from the q1 normal mode. Table 4.2.2 shows the $b_i * c_j$ multiplied by the corresponding integral that contributes to $|M_{ji}|^2$. As expected $b_0 * c_1$ has the largest contribution towards the transition moment for the anharmonic wavefunctions, but several anharmonic transitions given by other $b_i * c_j$ combinations make large contributions of approximately 10% that of $b_0 * c_1$.

See Appendix 1 for the Maple code that calculated the eigenvectors for the v=0 and v=1 anharmonic wavefunction, and Appendix 2 for the Maple code that used the calculated eigenvectors and the calculated v=0 to v=1 anharmonic vibrational frequency to calculate the square of the transition dipole function.

Table 4.2.1. This table lists, for each mode, the contributions from each harmonic wavefuction in the linear combination of harmonic wavefunctions to form the anharmonic wavefunctions. The harmonic frequencies required for these calculations came from the internal coordinate Hessian matrix. *Ab initio* results came from aug-cc-pVQZ and CCSD(T).

Anharmonic vibrational state	Harmonic vibrational state	q1	q2	q3
0	0	0.9913	0.9988	0.9999
	1	0.1264	0.0470	-0.0158
	2	0.0147	0.0026	0.0001
	3	0.0335	0.0127	-0.0042
Anharmonic vibrational state	**Harmonic vibrational state**	**q1**	**q2**	**q3**
1	0	-0.1255	-0.0471	0.0158
	1	0.9323	0.9902	0.9989
	2	0.3355	0.1313	-0.0443
	3	0.0492	0.0090	0.0007

Table 4.2.2. This table lists, for the q1 mode, the integral of the anharmonic wavefunctions with the x- and y-components of the dipole moment operator, multiplied by the products of b_i and c_j. The harmonic frequencies required for these calculations came from the internal coordinate Hessian matrix. *Ab initio* results came from aug-cc-pVQZ and CCSD(T).

		bi				
		0	1	2	3	
cj	0	-6.10E-04	-4.21E-04	-1.26E-05	1.14E-06	x
		8.61E-04	6.17E-04	1.78E-05	-3.00E-07	y
	1	2.46E-02	1.71E-03	5.10E-04	3.60E-04	x
		-3.59E-02	-2.41E-03	-7.54E-04	-5.06E-04	y
	2	2.27E-03	1.57E-03	1.18E-04	5.04E-04	x
		-3.19E-03	-2.33E-03	-1.66E-04	-7.53E-04	y
	3	-1.33E-05	7.17E-05	3.25E-05	5.41E-05	x
		3.48E-06	-1.01E-04	-4.86E-05	-7.60E-05	y

To test the maximum vibrational state for the linear combinations of harmonic wavefunctions, we varied the maximum vibrational state for each mode. The v=0 to v=1 anharmonic vibrational frequencies are listed in Table 4.2.3. Modes q2 and q3 were shown to converge using a maximum vibrational state of 5. Mode q1 was still changing at this vibrational state. We continued increased the maximum vibrational state for q1 until reaching maximum of v=9, by which point the frequency had changed from the v=8 by only 0.32 cm^{-1}. For all of the normal modes, the anharmonic v=0 to v=1 frequencies with the above maximum vibrational states are lower than the harmonic frequencies, as shown in Table 4.2.4. The biggest shift in frequency is from q1 with a decrease of 176.5 cm^{-1}, whereas the smallest decrease of less than 1 cm^{-1} is from the q3 mode.

Our calculated molar absorptivities, considering double harmonic approximation and differing amounts of anharmonicities, are given in Table 4.2.5. This table also includes, for comparison, the molar absorptivities of Lee which considered the double harmonic approximation with the TZ2P basis set (Lee 1993). Our double harmonic molar absorptivities differ greatly from Lee's double harmonic values, which must be mostly due to the difference in basis sets. This large difference shows the importance of performing calculations with our much larger aug-cc-pVQZ basis set compared to Lee's TZ2P basis set. Considering the electrical anharmonicity alone gives only a slightly different molar absorptivity than with our use of the double harmonic approximation, as the difference in molar absorptivity values are only around ±1 km/mol. The molar absorptivity from considering both mechanical and electrical anharmonicity resulted in the largest difference for q1 and q2 modes compared to our double harmonic

56

Table 4.2.3. Anharmonic frequency (cm^{-1}) of each mode, considering mechanical and electrical anharmonicity with different amounts of maximum vibrational states for the harmonic wavefunctions. *Ab initio* results came from aug-cc-pVQZ and CCSD(T).

Maximum v	$\nu1$	$\nu2$	$\nu3$
1	3253.28	1616.91	1544.78
2	2861.98	1588.99	1541.75
3	2857.90	1589.51	1541.83
4	2814.82	1586.36	1541.52
5	2793.66	1586.14	1541.51
6	2790.60		
7	2788.15		
8	2786.86		
9	2786.54		

Table 4.2.4. Anharmonic frequency (cm^{-1}) of each mode, considering mechanical and electrical anharmonicity. Values in parenthesis is the difference of the anharmonic frequency from the harmonic frequency for the v=0 to v=1 transition. Experimental frequencies are listed for comparison. The harmonic frequencies required for these calculations came from the internal coordinate Hessian matrix. *Ab initio* results came from aug-cc-pVQZ and CCSD(T).

	q1	q2	q3
Mechanical and Electrical Anharmonicity (q1: vmax=9; q2,q3: vmax=5)	2786.5	1586.1	1541.5
∆ from Harmonic Potential	(-176.5)	(-14.1)	(-0.7)
Experiment (Ruzi and Anderson 2015)	2694.5	1563.3	1500.9
Experiment (Johns, McKellar et al. 1983)	2684.0	1565.4	1500.8
Experiment (Jacox and Milligan 1973)	2717.0	1563.5	1505.0

Table 4.2.5. Molar Absorptivity (km/mol) of each mode. The anharmonic calculations specify maximum vibrational state of harmonic wavefunctions that were considered.

	q1	q2	q3
Lee	126	43	17
Double Harmonic	107.46	59.69	4.32
Electrical Anharmonicity (q1,q2,q3: vmax=3)	106.39	60.54	5.02
Mechanical & Electrical Anharmonicity (q1,q2,q3: vmax=3)	136.39	58.54	4.73
Mechanical & Electrical Anharmonicity (q1: vmax=9; q2,q3: vmax=5)	137.69	58.44	4.73

calculations. This large change in molar absorptivity values demonstrates the importance of including anharmonic effects for the vibrational analysis of the HNO molecule. Including larger harmonic vibrational states had a small but still important impact on all three modes, where the most impacted mode was mode 1.

Anderson measures the ratios of the integrated intensities of the observed vibrational infrared peaks, which are equal to the ratio of the vibrational molar absorptivities. Table 4.2.6 lists theoretical ratios from the molar absorptivities of mode 2 to mode 1 and of mode 3 to mode 1 from the molar absorptivities listed in Table 4.2.5, and also lists Anderson's experimental ratios for comparison (Anderson 2014). Our work has resulted in ratios much closer to Anderson's experimental work. Our anharmonic molar absorptivity ratios still are in need of improvement, which highlights the importance to consider coupling of normal modes.

4.3 Coupling

This chapter so far has discussed and explored the effects on frequency, eigenvectors, potential energy functions and dipole moment functions, and molar absorptivities with inclusion of anharmonic effects. The last topic we will briefly consider is the coupling of two or more normal modes. We explored the coupling between two modes. Figures 4.3.1, 4.3.2, and 4.3.3 show contour plots consisting of MP2, aug-cc-pVTZ potential energies of q1 with q2 coupling, q1 with q3 coupling, and q2 with q3 coupling, respectively. For this analysis only mechanical coupling was considered, and in the future electrical coupling will also need to be investigated for the HNO molecule. For each point on the potential energy graphs, the optimal HNO geometry was altered

Table 4.2.6. Molar absorptivity ratios, which are equal to the relative integrated intensities from an infrared spectrum.

	v2/v1	v3/v1
Lee	0.341	0.134
Double Harmonic	0.555	0.040
Electrical Anharmonicity (q1,q2,q3: vmax=3)	0.569	0.047
Mechanical & Electrical Anharmonicity (q1,q2,q3: vmax=3)	0.429	0.035
Mechanical & Electrical Anharmonicity (q1: vmax=9; q2,q3: vmax=5)	0.424	0.034
Anderson - Experimental	0.694	0.018
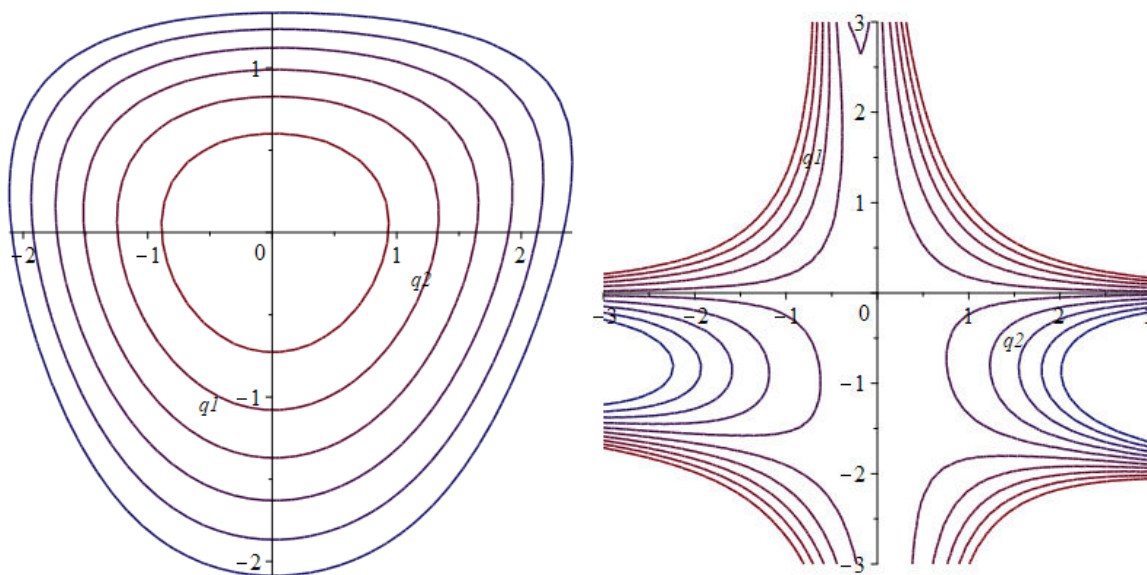
Figure 4.3.1. Potential energies contour plot of q1 vs. q2. *Left graph:* Full potential energy curve from the contributions of q1 and q2. Each line is 0.003 Ha apart. The higher red character of a line indicates a lower energy, and the higher blue character of a line indicates a higher energy. Spacing between lines is 0.003 Ha. *Right graph*: Coupling contributions alone to the potential energy. The higher red character of a line indicates a lowering of the energy, and the higher blue character indicates a raising of the energy. Spacing between lines is 0.0003 Ha. Energies are resultant from *ab initio* calculations with aug-cc-pVTZ, MP2.
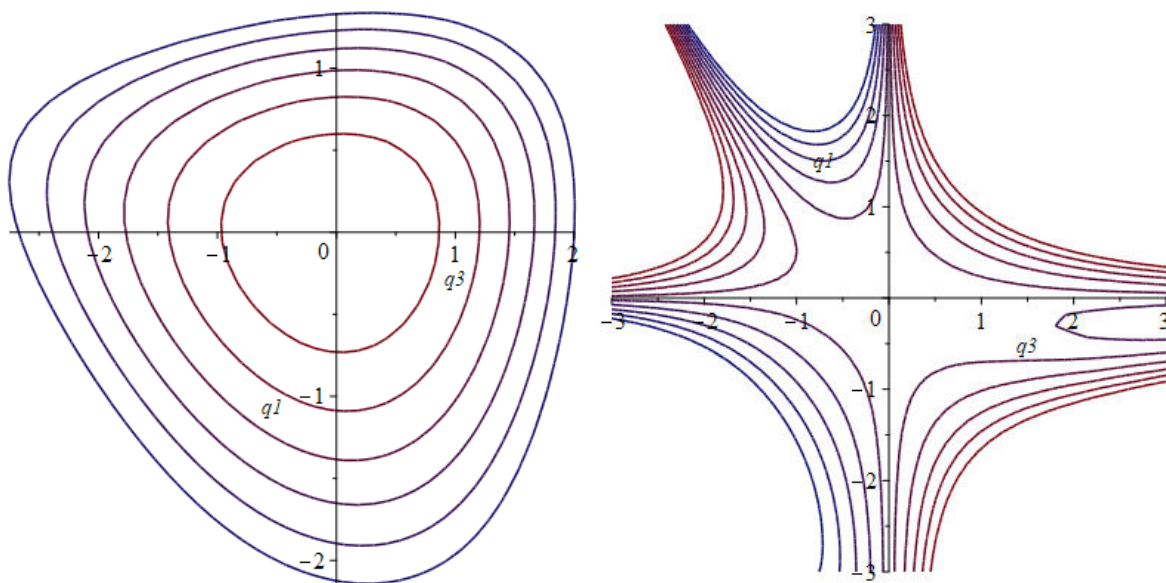
Figure 4.3.2. Potential energies contour plot of q1 vs. q3. *Left graph:* Full potential energy curve from the contributions of q1 and q3. Each line is 0.003 Ha apart. The higher red character of a line indicates a lower energy, and the higher blue character of a line indicates a higher energy. Spacing between lines is 0.003 Ha. *Right graph*: Coupling contributions alone to the potential energy. The higher red character of a line indicates a lowering of the energy, and the higher blue character indicates a raising of the energy. Spacing between lines is 0.0003 Ha. Energies are resultant from *ab initio* calculations with aug-cc-pVTZ, MP2.
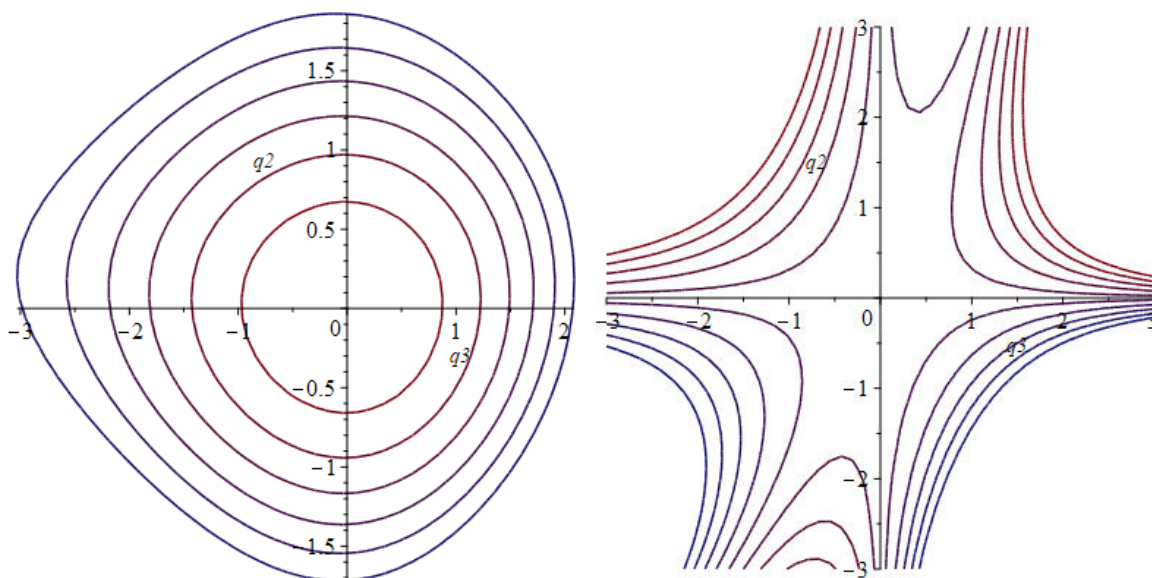
Figure 4.3.3. Potential energies contour plot of q2 vs. q3. *Left graph:* Full potential energy curve from the contributions of q2 and q3. Each line is 0.003 Ha apart. The higher red character of a line indicates a lower energy, and the higher blue character of a line indicates a higher energy. Spacing between lines is 0.003 Ha. *Right graph*: Coupling contributions alone to the potential energy. The higher red character of a line indicates a lowering of the energy, and the higher blue character indicates a raising of the energy. Spacing between lines is 0.0003 Ha. Energies are resultant from *ab initio* calculations with aug-cc-pVTZ, MP2.

by displacements along both normal modes before computing the potential energy of the new geometry.

The left graph in each of these figures show the behavior of the true potential energy, which has contributions from the harmonic quadratic force constant, the anharmonic effects, and possible coupling effects. These figures considered up to the fourth power of anharmonic and coupling contributions. The graph on the right subtracts the harmonic and anharmonic contributions, and any remaining effects to the potential energy are from the coupling contributions. The higher red character of a line indicates the coupling contributes a lowering of the potential energy, and the higher blue character of a line indicates the coupling contributes a raising of the energy. It is clear from these graphs that coupling is occurring from each combination of two normal modes. Future work can include a similar analysis to study the coupling between all three normal modes. Future work can also study the coupling at higher powers, as well as at different basis sets and theories. Including coupling contributions results in understanding more of the true behavior of these normal modes and should lead to more agreement between the theoretical molar absorptivity ratios and Anderson's experimental ratios.

Chapter 5

Conclusions and Future Work

5.1 Importance of Work

For Anderson to correctly understand the results of his experimental work with the *para*-hydrogen matrix doped with NO radicals and the reactions through which HNO molecules and NOH molecules are formed, accurate molar absorptivities for each HNO vibration are needed. Currently the only available HNO molar absorptivities were calculated using a small basis set and assumed the double harmonic approximation. Anderson's use of those previously computed molar absorptivities along with the peak intensities in his infrared spectra gives vastly large disagreements of the HNO concentration depending on whether he uses the HN stretching mode or the bending mode to calculate concentrations. This called our attention to explore how to improve the molar absorptivities.

5.2 Double Harmonic Results

Chapters 2 and 3 tested the double harmonic approximation with aug-cc-pVTZ and aug-cc-pVQZ basis sets and the Hartree Fock, MP2, CCSD, and CCSD(T) theories, and our results were compared to each other, as well as to previous results by Lee which were obtained from *ab initio* calculations using the smaller TZ2P basis set with the CCSD(T) theory (Lee 1993). The Hessian matrix was first calculated with respect to Cartesian coordinates. The diagonalization of this matrix provided the harmonic frequencies and eigenvectors to describe each normal mode. It was discovered that the q1 mode was most attributing to the stretch of the NH bond, while the q2 and q3 modes both had large effects on the NO bond stretch and the HNO bond

67

angle bend. Due to the close proximity of the frequencies of the q2 and q3 modes, coupling of these normal modes may be seen in spectroscopic data.

Isotopic substitution in computing the mass-weighted Hessian matrix gave us insight to the frequency shift of each normal mode when the ^{2}H, ^{15}N, or ^{18}0 isotopes are substituted into the molecule. The largest shift in frequencies, as expected due to the mass percentage increase of the isotope, was in substituting ^{2}H for ^{1}H. The ^{14}N to ^{15}N isotopic substitution was especially important to test due to both of these nitrogen isotopes being included in Anderson's experiments.

To reduce computational cost, we investigated completing the Hessian matrix through calculations with respect to internal coordinates. The Hessian matrix results proved to have minimal differences between the internal coordinate technique and the Cartesian coordinate technique. Future Hessian calculations for the HNO molecule are, therefore, recommended to be completed through the internal coordinate technique.

Lastly, the behavior of the *ab initio* potential energies and dipole moments indicated the breakdown of the double harmonic approximation with the HNO molecule.

5.3 Anharmonic Effects

Mechanical and electrical anharmonicities were considered by expansion of the potential energy functions and dipole moment functions, respectively. The largest shift in the molar absorptivity when including anharmonicities was for the q1 mode. Molar absorptivity ratios with including anharmonic effects agreed much more to Anderson's experimental results than the ratios from Lee's work. This proves the importance of

including larger basis sets and anharmonic effects in future work with the HNO molecule.

5.4 Conclusions

This work has shown that the TZ2P basis set that was used for previous molar absorptivity calculations does not consider enough basis functions to compute an accurate HNO molar absorptivity. In addition, even with the inclusion of larger basis sets, the double harmonic approximation is shown to break down for HNO.

With the inclusion of both mechanical and electrical anharmonicity effects, it was shown that there is an especially large anharmonicity in the q1 mode that describes the NH stretch, while the other modes are less anharmonic. As a result, we found that the amount of mode q1 harmonic functions required to describe the anharmonic wavefunction and energy levels of q1 must be substantially higher than the amount of harmonic wavefunctions for q2 and q3.

The theoretical isotopic substitutions of the atoms within HNO have shown the q2 and q3 shifts in frequencies to be very sensitive to the level of electron-electron correlation within the theory. Consideration of higher electron correlated theories should provide a convergence of the frequencies of each mode.

The contour plots have provided graphical evidence of coupling between the three modes. This coupling work was completed with aug-cc-pVTZ, MP2 energies. Similar work with aug-cc-pVQZ and CCSD(T) will provide a better understanding of the coupling between the modes within HNO.

5.5 Future Work

In addition to the earlier expressed importance of calculating Hessian matrices through internal coordinates in future work with HNO, it is also extremely important to consider coupling of normal modes in future work. The inclusion of coupling along with anharmonic effects will improve the molar absorptivities of the normal modes and the ratios of these molar absorptivities to be compared to experimental ratios.

References

Anderson, D. (2014). Professor of Chemical Physics. University of Wyoming, Laramie, WY. Personal communication.

Bak, K. L., J. Gauss, T. Helgaker, P. Jorgensen and J. Olsen (2000). "The accuracy of molecular dipole moments in standard electronic structure calculations." Chemical Physics Letters **319**(5-6): 563-568.

Benderskii, V. A., V. I. Goldanskii and D. E. Makarov (1993). "Quantum dynamics in low-temperature chemistry." Physics Reports **233**(4): 195-339.

Cohen, E. R., Cvitas, T., Frey, J. G., Holmstrom, B., Kuchitsu, K., Marquardt, R., Mills, I., Pavese, F., Quack, M., Stohner, J., Strauss, H. L., Takami, M., Thor, A. J. "Quantities, Units and Symbols in Physical Chemistry, IUPAC Green Book" 3rd ed. IUPAC & RSC Publishing: Cambridge, 2008.

Bozkaya, U., J. M. Turney, Y. Yamaguchi and H. F. Schaefer (2012). "The lowest-lying electronic singlet and triplet potential energy surfaces for the HNO-NOH system: Energetics, unimolecular rate constants, tunneling and kinetic isotope effects for the isomerization and dissociation reactions." Journal of Chemical Physics **136**(16).

Coriani, S., D. Marchesan, J. Gauss, C. Hattig, T. Helgaker and P. Jorgensen (2005). "The accuracy of ab initio molecular geometries for systems containing second-row atoms." Journal of Chemical Physics **123**(18).

Dalby, F. W. (1958). "The spectrum and structure of the HNO molecule." <u>Canadian Journal of Physics</u> **36**(10): 1336-&.

Jacox, M. E. and D. E. Milligan (1973). "Matrix-Isolation Study of Reaction of H atoms with NO - Infrared-Spectrum of HNO." <u>Journal of Molecular Spectroscopy</u> **48**(3): 536-559.

Johns, J. W. C., A. R. W. McKellar and E. Weinberger (1983). "The Infrared-Spectrum of HNO." <u>Canadian Journal of Physics</u> **61**(7): 1106-1119.

Kumada, T. (2003). "Experimental determination of the mechanism of the tunneling diffusion of H atoms in solid hydrogen: Physical exchange versus chemical reaction." <u>Physical Review B</u> **68**(5).

Kumada, T., M. Sakakibara, T. Nagasaka, H. Fukuta, J. Kumagai and T. Miyazaki (2002). "Absence of recombination of neighboring H atoms in highly purified solid parahydrogen: Electron spin resonance, electron-nuclear double resonance, and electron spin echo studies." <u>Journal of Chemical Physics</u> **116**(3): 1109-1119.

Lee, T. J. (1993). "A Coupled-Cluster Study of XNO (X=H,F,Cl) - An Investigation of Weak X-N Single Bonds." <u>Journal of Chemical Physics</u> **99**(12): 9783-9789.

Miranda, K. M., T. Katori, C. L. T. de Holding, L. Thomas, L. A. Ridnour, W. J. MeLendon, S. M. Cologna, A. S. Dutton, H. C. Champion, D. Mancardi, C. G. Tocchetti,

J. E. Saavedra, L. K. Keefer, K. N. Houk, J. M. Fukuto, D. A. Kass, N. Paolocci and D. A. Wink (2005). "Comparison of the NO and HNO donating properties of diazeniumdiolates: Primary amine adducts release HNO in vivo." Journal of Medicinal Chemistry **48**(26): 8220-8228.

Patrick, R. and D. M. Golden (1984). "KINETICS OF THE REACTIONS OF NH2 RADICALS WITH O-3 AND O-2." Journal of Physical Chemistry **88**(3): 491-495.

Ruzi, M. and D. T. Anderson (2015). "Quantum Diffusion-Controlled Chemistry: Reactions of Atomic Hydrogen with Nitric Oxide in Solid Parahydrogen." Journal of Physical Chemistry A **119**(50): 12270-12283.

Ulich, B. L., J. M. Hollis and L. E. Snyder (1977). "RADIO DETECTION OF NITROXYL (HNO) - 1ST INTERSTELLAR NO BOND." Astrophysical Journal **217**(2): L105-L108.

Appendices

Appendix 1

***APPENDIX* 1**

```
# Maple worksheet to fit potential energies to a 6th order polynomial.
# This worksheet then uses the force constants from the potential energy functions (not considering
    coupling force constants) in Hamiltonian matrix to calculate the anharmonic eigenvalues, the
    anharmonic v=0-->v=1 frequency from these eigenvalues, and eigenvector of each harmonic
    oscillator wavefunction that make up each overall anharmonic wavefunction.

# Each time this is run, we will need to provide:
# - the maximum vibrational levels we're considering for each normal mode (n1max, n2max, n3max)
# - the data file for xpts (amount of normal modes applied) and ypts for each mode (potential energies at
    those applied normal modes)
# - the Hessian frequencies for each mode (v1_freq, v2_freq, v3_freq)


#---------------------------------------------------------------------------------------------------------------

# restart Maple to clear the memory
restart;

# Load linear algebra package
with(linalg);
```

[*BlockDiagonal, GramSchmidt, JordanBlock, LUdecomp, QRdecomp, Wronskian, addcol,*   **(1)**
    addrow, adj, adjoint, angle, augment, backsub, band, basis, bezout, blockmatrix, charmat,
    charpoly, cholesky, col, coldim, colspace, colspan, companion, concat, cond, copyinto,
    crossprod, curl, definite, delcols, delrows, det, diag, diverge, dotprod, eigenvals, eigenvalues,
    eigenvectors, eigenvects, entermatrix, equal, exponential, extend, ffgausselim, fibonacci,
    forwardsub, frobenius, gausselim, gaussjord, geneqns, genmatrix, grad, hadamard, hermite,
    hessian, hilbert, htranspose, ihermite, indexfunc, innerprod, intbasis, inverse, ismith,
    issimilar, iszero, jacobian, jordan, kernel, laplacian, leastsqrs, linsolve, matadd, matrix,
    minor, minpoly, mulcol, mulrow, multiply, norm, normalize, nullspace, orthog, permanent,
    pivot, potential, randmatrix, randvector, rank, ratform, row, rowdim, rowspace, rowspan,
    rref, scalarmul, singularvals, smith, stackmatrix, submatrix, subvector, sumbasis, swapcol,
    swaprow, sylvester, toeplitz, trace, transpose, vandermonde, vecpotent, vectdim, vector,
    wronskian]

```
# load the fitting package
with(stats); with(plots); with(PolynomialTools);
```
        [*anova, describe, fit, importdata, random, statevalf, statplots, transform*]

[*animate, animate3d, animatecurve, arrow, changecoords, complexplot, complexplot3d,*
    conformal, conformal3d, contourplot, contourplot3d, coordplot, coordplot3d, densityplot,
    display, dualaxisplot, fieldplot, fieldplot3d, gradplot, gradplot3d, implicitplot, implicitplot3d,
    inequal, interactive, interactiveparams, intersectplot, listcontplot, listcontplot3d,
    listdensityplot, listplot, listplot3d, loglogplot, logplot, matrixplot, multiple, odeplot, pareto,
    plotcompare, pointplot, pointplot3d, polarplot, polygonplot, polygonplot3d,
    polyhedra_supported, polyhedraplot, rootlocus, semilogplot, setcolors, setoptions,
    setoptions3d, shadebetween, spacecurve, sparsematrixplot, surfdata, textplot, textplot3d,
    tubeplot]

$[AnnihilatingPolynomial, CoefficientList, CoefficientVector, FromCoefficientList,$ **(2)**
    $FromCoefficientVector, GcdFreeBasis, GreatestFactorialFactorization, Homogenize,$
    $Hurwitz, IsHomogeneous, IsSelfReciprocal, MinimalPolynomial, PDEToPolynomial,$
    $PolynomialToPDE, ShiftEquivalent, ShiftlessDecomposition, Shorten, Shorter, Sort, Split,$
    $Splits, SquareFreePart, Translate]$

#---

Parameters to set. n1, n2, n3 represents the vibrational energy levels for each mode.
Set maximum n1 (n1max), maximum n2 (n2max), maximum n3 (n3max).
$n1max := 3; n2max := 0; n3max := 0$

$$n1max := 3$$
$$n2max := 0$$
$$n3max := 0 \qquad \textbf{(3)}$$

$n1 := [seq(seq(seq(n1, n1 = 0..n1max), n2 = 0..n2max), n3 = 0..n3max)]$
$$n1 := [0, 1, 2, 3] \qquad \textbf{(4)}$$

$n2 := [seq(seq(seq(n2, n1 = 0..n1max), n2 = 0..n2max), n3 = 0..n3max)]$
$$n2 := [0, 0, 0, 0] \qquad \textbf{(5)}$$

$n3 := [seq(seq(seq(n3, n1 = 0..n1max), n2 = 0..n2max), n3 = 0..n3max)]$
$$n3 := [0, 0, 0, 0] \qquad \textbf{(6)}$$

number of points (nops) here represents the size of each side of the matrix
$n1size := nops(n1); n2size := nops(n2); n3size := nops(n3);$
$$n1size := 4$$
$$n2size := 4$$
$$n3size := 4 \qquad \textbf{(7)}$$
#---

these are the x values; x=normal mode
$xpts :=$
    $readdata("C:/Users/Kirano/Documents/Research/TheoriesAndBasisSets/ccsd(t)$
    $/aug-cc-pvqz/InternalCoordinates/q1/V-vs-q/q-range.txt", 1)$
$xpts := [-5.0, -4.5, -4.0, -3.5, -3.0, -2.5, -2.0, -1.5, -1.0, -0.5, 0., 0.5, 1.0, 1.5, 2.0,$ **(8)**
    $2.5, 3.0, 3.5, 4.0, 4.5, 5.0]$

$nops(xpts);$
$$21 \qquad \textbf{(9)}$$

$Digits := 13$
$$Digits := 13 \qquad \textbf{(10)}$$

these are the y values; y=Potential Energy
$ypts\_v1 :=$

readdata("C:/Users/Kirano/Documents/Research/TheoriesAndBasisSets/ccsd(t)/aug-cc-pvqz/InternalCoordinates/q1/V—vs—q/PotE.txt", 1)

$ypts\_v1 := [-130.2684311470, -130.2809089089, -130.2927740085, -130.3037478566,$ **(11)**
    $-130.3136076294, -130.3221863270, -130.3293656603, -130.3350629274,$
    $-130.3392144984, -130.3417597355, -130.3426293322, -130.3417410978,$
    $-130.3390041430, -130.3343301564, -130.3276487796, -130.3189235390,$
    $-130.3081652155, -130.2954403905, -130.2808734052, -130.2646393655,$
    $-130.2469443680]$

$ypts\_v2 :=$
    readdata("C:/Users/Kirano/Documents/Research/TheoriesAndBasisSets/ccsd(t)/aug-cc-pvqz/InternalCoordinates/q2/V—vs—q/PotE.txt", 1)

$ypts\_v2 := [-130.2016986454, -130.2331479762, -130.2597169002, -130.2818188423,$ **(12)**
    $-130.2998528166, -130.3142007879, -130.3252257596, -130.3332704432,$
    $-130.3386563754, -130.3416833821, -130.3426293322, -130.3417501428,$
    $-130.3392800269, -130.3354319790, -130.3303985020, -130.3243525800,$
    $-130.3174489357, -130.3098256174, -130.3016059945, -130.2929012902,$
    $-130.2838138394]$

$ypts\_v3 :=$
    readdata("C:/Users/Kirano/Documents/Research/TheoriesAndBasisSets/ccsd(t)/aug-cc-pvqz/InternalCoordinates/q3/V—vs—q/PotE.txt", 1)

$ypts\_v3 := [-129.5172460596, -129.7903199620, -129.9784445791, -130.1078961035,$ **(13)**
    $-130.1963467288, -130.2558932730, -130.2949542699, -130.3194728555,$
    $-130.3336931811, -130.3406729555, -130.3426293322, -130.3411763569,$
    $-130.3374899417, -130.3324235075, -130.3265900330, -130.3204216919,$
    $-130.3142147896, -130.3081647185, -130.3023935636, -130.2969718387,$
    $-130.2919352895]$

 # "a" value can be set to the minimum value of the energy (all modes should have the same min E), a.k.
    a. the optimum energy (OptE), which is the energy at x=0.
$\min(ypts\_v1); \min(ypts\_v2); \min(ypts\_v3)$
$$-130.3426293322$$
$$-130.3426293322$$
$$-130.3426293322 \qquad \textbf{(14)}$$
$OptE := \min(ypts\_v1);$
$$OptE := -130.3426293322 \qquad \textbf{(15)}$$

$nops(ypts\_v1); nops(ypts\_v2); nops(ypts\_v3)$
$$21$$
$$21$$
$$21 \qquad \textbf{(16)}$$

 # In atomic units : hbar = [1 Ha · a.u.time] = constant, Eigenvalue = lambda = [a.u.time^{-2}] = freq^2; ((
    in *atomic units, freq = [a.u.time^{-1}])).*
$hbar := 1$

$$\hbar := 1 \tag{17}$$

Give the frequencies (in cm-1) of the three modes
v1_freq := 1542.18025 ; *v2_freq* := 1600.228641 ; *v3_freq* := 2963.03259

$$v1\_freq := 1542.18025$$
$$v2\_freq := 1600.228641$$
$$v3\_freq := 2963.03259 \tag{18}$$

$$w1 := \left(\frac{v1\_freq}{219474.63} \right)$$

$$w1 := 0.007026690283063 \tag{19}$$

$$w2 := \left(\frac{v2\_freq}{219474.63} \right)$$

$$w2 := 0.007291178214994 \tag{20}$$

$$w3 := \left(\frac{v3\_freq}{219474.63} \right)$$

$$w3 := 0.01350056992920 \tag{21}$$

Define the results of the integral $<v1|q^n|v2>$, where q is defined using ladder operators.
q0 is $<v1|q^0|v2>$, q1 is $<v1|q^1|v2>$, ... Define q0, q1, q2, q3, q4.

$q0 := (n1, n2) \rightarrow$ **if** $n1 = n2$ **then** 1 **else** 0 **fi**

$$q0 := (n1, n2) \mapsto \text{if } n1 = n2 \text{ then } 1 \text{ else } 0 \text{ end if} \tag{22}$$

$q1 := (n1, n2) \rightarrow$ **if** $n1 < 0$ **then** 0 **elif** $n2 < 0$ **then** 0 **elif** $\text{abs}(n1 - n2) = 1$ **then** $\text{sqrt}\left(\frac{\max(n1, n2)}{2} \right)$

   else 0 **fi**

$$q1 := (n1, n2) \mapsto \text{if } n1 < 0 \text{ then } 0 \text{ elif } n2 < 0 \text{ then } 0 \text{ elif } |n1 - n2| = 1 \text{ then } \sqrt{\frac{\max(n1, n2)}{2}} \tag{23}$$

   else 0 **end if**

$q2 := (n1, n2) \rightarrow add(q1(n1, i) \cdot q1(i, n2), i = n2 - 1 .. n2 + 1)$

$$q2 := (n1, n2) \mapsto add(q1(n1, i)\, q1(i, n2), i = n2 - 1 .. n2 + 1) \tag{24}$$

$q3 := (n1, n2) \rightarrow add(q2(n1, i) \cdot q1(i, n2), i = n2 - 1 .. n2 + 1)$

$$q3 := (n1, n2) \mapsto add(q2(n1, i)\, q1(i, n2), i = n2 - 1 .. n2 + 1) \tag{25}$$

$q4 := (n1, n2) \rightarrow add(q3(n1, i) \cdot q1(i, n2), i = n2 - 1 .. n2 + 1)$

$$q4 := (n1, n2) \mapsto add(q3(n1, i)\, q1(i, n2), i = n2 - 1 .. n2 + 1) \tag{26}$$

$q5 := (n1, n2) \rightarrow add(q4(n1, i) \cdot q1(i, n2), i = n2 - 1 .. n2 + 1)$

$$q5 := (n1, n2) \mapsto add(q4(n1, i)\, q1(i, n2), i = n2 - 1 .. n2 + 1) \tag{27}$$

$q6 := (n1, n2) \rightarrow add(q5(n1, i) \cdot q1(i, n2), i = n2 - 1 .. n2 + 1)$
$$q6 := (n1, n2) \mapsto add(q5(n1, i)\, q1(i, n2), i = n2 - 1 .. n2 + 1) \tag{28}$$

Quadratic force constant is equal to $\dfrac{hbar \cdot \text{sqrt}(eigval)}{2}$, where each eigenvalue is equal

to $\left(\dfrac{freq}{219474.63} \right)^2$, and 219474.63 converts to Ha from cm − 1.

$v1\_Eqn := OptE + \left(\dfrac{hbar \cdot v1\_freq}{2} \cdot \dfrac{1}{219474.63} \right) \cdot x^2 + c \cdot x^3 + d \cdot x^4 + e \cdot x^5 + f \cdot x^6$

$$v1\_Eqn := -130.3426293322 + 0.003513345141532\, x^2 + c\, x^3 + d\, x^4 + e\, x^5 + f\, x^6 \tag{29}$$

recalculate the fit
$v1\_Func := rhs(\,fit[leastsquare[[x, y], y = v1\_Eqn]]([xpts, ypts\_v1]));$

$$v1\_Func := -130.3426293322 + 0.003513345141532\, x^2 + 0.0001072187911663\, x^3 \tag{30}$$
$$+ 4.089828590046\ 10^{-6}\, x^4 - 8.609888690258\ 10^{-7}\, x^5 - 3.505288048860\ 10^{-7}\, x^6$$

$printf(\text{"OptE, linear coefficient (should be zero), b, c, d, e , f are:"}) : const\_v1 :=$
$\quad CoefficientList(v1\_Func, x)$

```
OptE, linear coefficient (should be zero), b, c, d, e , f are:
```

$$const\_v1 := [-130.3426293322,\ 0,\ 0.003513345141532,\ 0.0001072187911663, \tag{31}$$
$$4.089828590046\ 10^{-6},\ -8.609888690258\ 10^{-7},\ -3.505288048860\ 10^{-7}]$$

$const\_v1_1$
$$-130.3426293322 \tag{32}$$

$const\_v1_2$
$$0 \tag{33}$$

$const\_v1_3$
$$0.003513345141532 \tag{34}$$

$const\_v1_4$
$$0.0001072187911663 \tag{35}$$

$const\_v1_5$
$$4.089828590046\ 10^{-6} \tag{36}$$

$const\_v1_6$
$$-8.609888690258\ 10^{-7} \tag{37}$$

$const\_v1_7$
$$-3.505288048860\ 10^{-7} \tag{38}$$

Calculate the deviations between the actual energies and the predicted ones
AND isolate the Maximum Absolute Deviation

$v1\_dev := [seq(ypts\_v1[i] - subs(x = xpts[i], v1\_Func), i = 1 .. nops(xpts))]; \max(seq(\text{abs}(\%[i]), i$

$= 1 ..nops(xpts)));$

$v1\_dev := [-2.8149 \ 10^{-6}, -9.6464 \ 10^{-6}, 0.0000109213, 0.0000184310, 0.0000115430,$
$\quad 1.6302 \ 10^{-6}, -2.5135 \ 10^{-6}, -8.6 \ 10^{-9}, 4.1072 \ 10^{-6}, 4.3857 \ 10^{-6}, 0., -3.7274 \ 10^{-6},$
$\quad 1.7470 \ 10^{-6}, 0.0000221118, 0.0000539698, 0.0000819928, 0.0000825827, 0.0000363007,$
$\quad -0.0000491754, -0.0001031944, 0.0000604467]$

$$0.0001031944 \tag{39}$$

Calculate the Mean Absolute Deviation

$$\frac{add(\text{abs}(v1\_dev[i]), i = 1 ..nops(xpts))}{nops(xpts)}$$

$$0.00002672621428571 \tag{40}$$

Calculate the Root Mean Square Deviation

$$\text{sqrt}\left(\frac{\left(sum(\ (v1\_dev[i])^2, i = 1 ..nops(xpts))\ \right)}{nops(xpts)} \right)$$

$$0.00004125325932481 \tag{41}$$

$v2\_Eqn := OptE + \left(\dfrac{hbar \cdot v2\_freq}{2} \cdot \dfrac{1}{219474.63} \right) \cdot x^2 + c \cdot x^3 + d \cdot x^4 + e \cdot x^5 + f \cdot x^6$

$$v2\_Eqn := -130.3426293322 + 0.003645589107497\ x^2 + c\ x^3 + d\ x^4 + e\ x^5 + f\ x^6 \tag{42}$$

recalculate the fit
$v2\_Func := rhs(\ fit[\ leastsquare[\ [x, y], y = v2\_Eqn]](\ [xpts, ypts\_v2]));$

$$v2\_Func := -130.3426293322 + 0.003645589107497\ x^2 - 0.0003246477232452\ x^3 \tag{43}$$
$$\quad + 0.00001465079109528\ x^4 - 1.547178080177 \ 10^{-7} x^5 - 2.713685859482 \ 10^{-8} x^6$$

$printf(\text{"OptE, linear coefficient (should be zero), b, c, d, e , f are:"}) : const\_v2 :=$
$\quad CoefficientList(v2\_Func, x)$
OptE, linear coefficient (should be zero), b, c, d, e , f are:

$const\_v2 := [-130.3426293322, 0, 0.003645589107497, -0.0003246477232452, \tag{44}$
$\quad 0.00001465079109528, -1.547178080177 \ 10^{-7}, -2.713685859482 \ 10^{-8}]$

$const\_v2_1$

$$-130.3426293322 \tag{45}$$

$const\_v2_2$

$$0 \tag{46}$$

$const\_v2_3$

$$0.003645589107497 \tag{47}$$

$const\_v2_4$

$$-0.0003246477232452 \tag{48}$$

82

$const\_v2_5$

$$0.00001465079109528 \qquad \textbf{(49)}$$

$const\_v2_6$

$$-1.547178080177 \ 10^{-7} \qquad \textbf{(50)}$$

$const\_v2_7$

$$-2.713685859482 \ 10^{-8} \qquad \textbf{(51)}$$

Calculate the deviations between the actual energies and the predicted ones
AND isolate the Maximum Absolute Deviation

$v2\_dev := [seq(ypts\_v2[i] - subs(x = xpts[i], v2\_Func), i = 1 ..nops(xpts))]; max(seq(abs(\%[i]), i = 1 ..nops(xpts)))$;

$v2\_dev := [-6.2305 \ 10^{-6}, 6.7530 \ 10^{-6}, 7.6711 \ 10^{-6}, 2.8420 \ 10^{-6}, -3.8026 \ 10^{-6},$
$\qquad -9.7888 \ 10^{-6}, -0.0000135925, -0.0000144080, -0.0000120584, -6.9483 \ 10^{-6}, 0.,$
$\qquad 7.4626 \ 10^{-6}, 0.0000138949, 0.0000177782, 0.0000179307, 0.0000138789, 6.2481 \ 10^{-6},$
$\qquad -2.8695 \ 10^{-6}, -9.6526 \ 10^{-6}, -8.5176 \ 10^{-6}, 7.4927 \ 10^{-6}]$

$$0.0000179307 \qquad \textbf{(52)}$$

Calculate the Mean Absolute Deviation

$$\frac{add(abs(v2\_dev[i]), i = 1 ..nops(xpts))}{nops(xpts)}$$

$$9.039095238095 \ 10^{-6} \qquad \textbf{(53)}$$

Calculate the Root Mean Square Deviation

$$sqrt\left(\frac{\left(sum((v2\_dev[i])^2, i = 1 ..nops(xpts))\right)}{nops(xpts)} \right)$$

$$0.00001022543070636 \qquad \textbf{(54)}$$

--

$v3\_Eqn := OptE + \left(\frac{hbar \cdot v3\_freq}{2} \cdot \frac{1}{219474.63} \right) \cdot x^2 + c \cdot x^3 + d \cdot x^4 + e \cdot x^5 + f \cdot x^6$

$$v3\_Eqn := -130.3426293322 + 0.006750284964599 \ x^2 + c \ x^3 + d \ x^4 + e \ x^5 + f x^6 \qquad \textbf{(55)}$$

recalculate the fit
$v3\_Func := rhs(fit[leastsquare[[x, y], y = v3\_Eqn]]([xpts, ypts\_v3]))$;

$v3\_Func := -130.3426293322 + 0.006750284964599 \ x^2 - 0.001591041803368 \ x^3 \qquad \textbf{(56)}$
$\qquad + 0.0002594445982952 \ x^4 - 0.00005986640415720 \ x^5 + 6.830689208016 \ 10^{-6} x^6$

$printf($"OptE, linear coefficient (should be zero), b, c, d, e , f are:"$) : const\_v3 :=$
$\qquad CoefficientList(v3\_Func, x)$
OptE, linear coefficient (should be zero), b, c, d, e , f are:

$const\_v3 := [-130.3426293322, 0, 0.006750284964599, -0.001591041803368,$ **(57)**
    $0.0002594445982952, -0.00005986640415720, 6.830689208016\ 10^{-6}]$

$const\_v3_1$

$$-130.3426293322 \qquad\qquad\text{(58)}$$

$const\_v3_2$

$$0 \qquad\qquad\text{(59)}$$

$const\_v3_3$

$$0.006750284964599 \qquad\qquad\text{(60)}$$

$const\_v3_4$

$$-0.001591041803368 \qquad\qquad\text{(61)}$$

$const\_v3_5$

$$0.0002594445982952 \qquad\qquad\text{(62)}$$

$const\_v3_6$

$$-0.00005986640415720 \qquad\qquad\text{(63)}$$

$const\_v3_7$

$$6.830689208016\ 10^{-6} \qquad\qquad\text{(64)}$$

 # Calculate the deviations between the actual energies and the predicted ones
 # AND isolate the Maximum Absolute Deviation

$v3\_dev := [seq(ypts\_v3[i] - subs(x = xpts[i], v3\_Func), i = 1\,..nops(xpts))]; \max(seq(abs(\%[i]), i$
    $= 1\,..nops(xpts)));$
$v3\_dev := [0.0017810173, -0.0029468805, -0.0013459998, 0.0008938364, 0.0020297889,$
    $0.0020382182, 0.0014415854, 0.0007527148, 0.0002686826, 0.0000517325, 0.,$
    $-0.0000501669, -0.0002262616, -0.0005491840, -0.0009060591, -0.0010774873,$
    $-0.0008269421, -0.0000570280, 0.0009647623, 0.0013093176, -0.0009827358]$

$$0.0029468805 \qquad\qquad\text{(65)}$$

 # Calculate the Mean Absolute Deviation

$$\frac{add(abs(v3\_dev[i]), i = 1\,..nops(xpts))}{nops(xpts)}$$

$$0.0009762095761905 \qquad\qquad\text{(66)}$$

 # Calculate the Root Mean Square Deviation

$$\text{sqrt}\left(\frac{\left(sum((v3\_dev[i])^2, i = 1\,..nops(xpts)) \right)}{nops(xpts)} \right)$$

$$0.001236276039002 \qquad\qquad\text{(67)}$$

 # --
    --

#Non-coupling anharmonic force constants. Ex: k300 is the 3rd order force constant for mode 1, k030 is

"" for mode 2, etc.

$k300 := const\_v1_4$

$$k300 := 0.0001072187911663 \tag{68}$$

$k400 := const\_v1_5$

$$k400 := 4.089828590046 \ 10^{-6} \tag{69}$$

$k500 := const\_v1_6$

$$k500 := -8.609888690258 \ 10^{-7} \tag{70}$$

$k600 := const\_v1_7$

$$k600 := -3.505288048860 \ 10^{-7} \tag{71}$$

$k030 := const\_v2_4$

$$k030 := -0.0003246477232452 \tag{72}$$

$k040 := const\_v2_5$

$$k040 := 0.00001465079109528 \tag{73}$$

$k050 := const\_v2_6$

$$k050 := -1.547178080177 \ 10^{-7} \tag{74}$$

$k060 := const\_v2_7$

$$k060 := -2.713685859482 \ 10^{-8} \tag{75}$$

$k003 := const\_v3_4$

$$k003 := -0.001591041803368 \tag{76}$$

$k004 := const\_v3_5$

$$k004 := 0.0002594445982952 \tag{77}$$

$k005 := const\_v3_6$

$$k005 := -0.00005986640415720 \tag{78}$$

$k006 := const\_v3_7$

$$k006 := 6.830689208016 \ 10^{-6} \tag{79}$$

--

Define the harmonic component of the Hamiltonian matrix

$h\_harm := matrix(4, 4, [seq(seq(q0(n1[i], n1[j]) \cdot q0(n2[i], n2[j]) \cdot q0(n3[i], n3[j]) \cdot (w1 \cdot (n1[i]$
    $+ 0.5) + w2 \cdot (n2[i] + 0.5) + w3 \cdot (n3[i] + 0.5)), j = 1..4), i = 1..4)]);$

$h\_harm :=$ $\tag{80}$

$$\begin{bmatrix} 0.01390921921363 & 0. & 0. & 0. \\ 0. & 0.02093590949669 & 0. & 0. \\ 0. & 0. & 0.02796259977976 & 0. \\ 0. & 0. & 0. & 0.03498929006282 \end{bmatrix}$$

Define the anharmonic contributions from mode 1 alone

$h\_q1 := matrix(4, 4, [seq(seq(q0(n2[i], n2[j]) \cdot q0(n3[i], n3[j]) \cdot (q3(n1[i], n1[j]) \cdot k300$

$$+ q4(n1[i], n1[j]) \cdot k400 + q5(n1[i], n1[j]) \cdot k500 + q6(n1[i], n1[j]) \cdot k600), j = 1 .. 4), i = 1 .. 4)$$
]);

$h\_q1 := \big[\big[2.410129933373 \ 10^{-6}, 0.00007879973924530 \sqrt{2}, 4.163018357585 \ 10^{-6} \sqrt{2},$ **(81)**

$0.00002572846170530 \sqrt{2} \sqrt{6} \big],$

$\big[0.00007879973924530 \sqrt{2}, 0.00001073616664854, 0.0003119702487224,$

$5.623880910991 \ 10^{-6} \sqrt{6} \big],$

$\big[4.163018357585 \ 10^{-6} \sqrt{2}, 0.0003119702487224, 0.00002344479102392,$

$0.0002310180373045 \sqrt{6} \big],$

$\big[0.00002572846170530 \sqrt{2} \sqrt{6}, 5.623880910991 \ 10^{-6} \sqrt{6}, 0.0002310180373045 \sqrt{6},$

$0.00003527807098620 \big]\big]$

Define the anharmonic contributions from mode 2 alone

$h\_q2 := matrix(4, 4, [seq(seq(q0(n1[i], n1[j]) \cdot q0(n3[i], n3[j]) \cdot (q3(n2[i], n2[j]) \cdot k030$
    $+ q4(n2[i], n2[j]) \cdot k040 + q5(n2[i], n2[j]) \cdot k050 + q6(n2[i], n2[j]) \cdot k060), j = 1 .. 4), i = 1 .. 4)$
]);

$h\_q2 := [[0.00001093721171159, 0., 0., 0.],$ **(82)**

$[0., 0.00001093721171159, 0., 0.],$

$[0., 0., 0.00001093721171159, 0.],$

$[0., 0., 0., 0.00001093721171159]]$

Define the anharmonic contributions from mode 3 alone

$h\_q3 := matrix(4, 4, [seq(seq(q0(n1[i], n1[j]) \cdot q0(n2[i], n2[j]) \cdot (q3(n3[i], n3[j]) \cdot k003$
    $+ q4(n3[i], n3[j]) \cdot k004 + q5(n3[i], n3[j]) \cdot k005 + q6(n3[i], n3[j]) \cdot k006), j = 1 .. 4), i = 1 .. 4)$
]);

$h\_q3 :=$ **(83)**

$[[0.0002073909909864, 0., 0., 0.],$

$[0., 0.0002073909909864, 0., 0.],$

$[0., 0., 0.0002073909909864, 0.],$

$[0., 0., 0., 0.0002073909909864]]$

# Eigenvalues
eigenvalues(h_harm);

   $0.0139092192136300, 0.0209359094966900, 0.0279625997797600, 0.0349892900628200$ **(84)**

Eigenvalues of the anharmonic vibrational states
$eigval := eigenvalues(h\_harm + h\_q1 + h\_q2 + h\_q3);$

$eigval := 0.0141278182943811, 0.0211529248120400, 0.0281728715983544,$ **(85)**

   0.0352885858175147

Calculate the ANharmonic frequency for the normal mode that included excited states.

$v\_anharm\_freq := (eigval[2] - eigval[1]) \cdot 219474.63$

$$v\_anharm\_freq := 1541.83265367378 \qquad (86)$$

--

Eigenvectors for each eigenvalue

For a harmonic wavefunction, each eigenvalue should have total population in one vibrational state. Reconfirm using command below.

$vex\_harm := eigenvectors(h\_harm)$

$$vex\_harm := \left[0.03498929006282, 1, \left\{\left[\begin{array}{cccc} 0 & 0 & 0 & 1 \end{array}\right]\right\}\right], \left[0.01390921921363, 1, \qquad (87)\right.$$
$$\left\{\left[\begin{array}{cccc} 1 & 0 & 0 & 0 \end{array}\right]\right\}\right], \left[0.02093590949669, 1, \left\{\left[\begin{array}{cccc} 0 & 1 & 0 & 0 \end{array}\right]\right\}\right], \left[0.02796259977976, 1,\right.$$
$$\left\{\left[\begin{array}{cccc} 0 & 0 & 1 & 0 \end{array}\right]\right\}\right]$$

$$vexharm := \left[0.03498929006282, 1, \left\{\left[\begin{array}{cccc} 0 & 0 & 0 & 1 \end{array}\right]\right\}\right], \left[0.01390921921363, 1, \qquad (88)\right.$$
$$\left\{\left[\begin{array}{cccc} 1 & 0 & 0 & 0 \end{array}\right]\right\}\right], \left[0.02093590949669, 1, \left\{\left[\begin{array}{cccc} 0 & 1 & 0 & 0 \end{array}\right]\right\}\right], \left[0.02796259977976, 1,\right.$$
$$\left\{\left[\begin{array}{cccc} 0 & 0 & 1 & 0 \end{array}\right]\right\}\right]$$

For an anharmonic wavefunction, each eigenvalue has population in all vibrational states, but has an overwhelming population in the vibrational state describing the eigenvalue.

$vex\_anharm := eigenvectors(h\_harm + h\_q1 + h\_q2 + h\_q3)$

$$vex\_anharm := \left[0.02817287159839, 1, \qquad (89)\right.$$
$$\{[-0.0002616512585637, -0.04417870346862, -0.9958318137024,$$
$$0.07979456445536]\}], \left[0.02115292481207, 1,\right.$$
$$\{[0.01582213462534, 0.9988943860429, -0.04426256023948,$$
$$0.0007009639895876]\}], \left[0.01412781829437, 1,\right.$$
$$\{[0.9998658167623, -0.01583004563139, 0.0001020009946264,$$
$$-0.004212804580395]\}], \left[0.03528858581751, 1,\right.$$
$$\left\{\left[\begin{array}{cccc} 0.004235571484453 & 0.002767191495755 & 0.07974844308818 & 0.9968021811827 \end{array}\right]\right\}\right]$$

------------------------END--

Appendix 2

APPENDIX 2

Maple worksheet that uses the 5th order dipole moment function for each vector to calculate transition dipole moments of each normal mode using the overall HARMONIC wavefunction for each mode, that was determined in the "Hamiltonian-Anharmonic-NoCoupling" Maple Sheet.

Must provide correct:
-eigenvectors that were found in "Hamiltonian-Anharmonic-NoCoupling" Maple Sheet.
-the ANHARMONIC vibrational frequencies (in cm-1) for each mode, which were calculated from the energy difference from the ground state to the first excited state in "Hamiltonian-Anharmonic-NoCoupling" Maple Sheet.
-the maximum vibrational state for each mode (n1max for mode 1, n2max for mode 2, n3max for mode 3). Since we are not looking at coupling, only one nmax should have an excited maximum vibrational state, while the others have nmax of zero.

When looking at multiple vibrational states of a certain mode while the others stay at ground state, expect the other Molar Adsorptivity from the other modes to be essentially zero. A recalculation must be completed using this code by changing which mode has excited states for the Transition Dipole Moment of that normal mode, and the Molar Absorptivity of that normal mode.

--

restart Maple to clear the memory
restart;

# Load linear algebra package
with(linalg);

[*BlockDiagonal, GramSchmidt, JordanBlock, LUdecomp, QRdecomp, Wronskian, addcol,* **(1)**
    addrow, adj, adjoint, angle, augment, backsub, band, basis, bezout, blockmatrix, charmat,
    charpoly, cholesky, col, coldim, colspace, colspan, companion, concat, cond, copyinto,
    crossprod, curl, definite, delcols, delrows, det, diag, diverge, dotprod, eigenvals, eigenvalues,
    eigenvectors, eigenvects, entermatrix, equal, exponential, extend, ffgausselim, fibonacci,
    forwardsub, frobenius, gausselim, gaussjord, geneqns, genmatrix, grad, hadamard, hermite,
    hessian, hilbert, htranspose, ihermite, indexfunc, innerprod, intbasis, inverse, ismith,
    issimilar, iszero, jacobian, jordan, kernel, laplacian, leastsqrs, linsolve, matadd, matrix,
    minor, minpoly, mulcol, mulrow, multiply, norm, normalize, nullspace, orthog, permanent,
    pivot, potential, randmatrix, randvector, rank, ratform, row, rowdim, rowspace, rowspan,
    rref, scalarmul, singularvals, smith, stackmatrix, submatrix, subvector, sumbasis, swapcol,
    swaprow, sylvester, toeplitz, trace, transpose, vandermonde, vecpotent, vectdim, vector,
    wronskian]

# load the fitting package
with(stats); with(plots); with(PolynomialTools);
          [*anova, describe, fit, importdata, random, statevalf, statplots, transform*]

[*animate, animate3d, animatecurve, arrow, changecoords, complexplot, complexplot3d,*
    conformal, conformal3d, contourplot, contourplot3d, coordplot, coordplot3d, densityplot,
    display, dualaxisplot, fieldplot, fieldplot3d, gradplot, gradplot3d, implicitplot, implicitplot3d,
    inequal, interactive, interactiveparams, intersectplot, listcontplot, listcontplot3d,
    listdensityplot, listplot, listplot3d, loglogplot, logplot, matrixplot, multiple, odeplot, pareto,

plotcompare, pointplot, pointplot3d, polarplot, polygonplot, polygonplot3d,
polyhedra_supported, polyhedraplot, rootlocus, semilogplot, setcolors, setoptions,
setoptions3d, shadebetween, spacecurve, sparsematrixplot, surfdata, textplot, textplot3d,
tubeplot]

[*AnnihilatingPolynomial, CoefficientList, CoefficientVector, FromCoefficientList,*   **(2)**
FromCoefficientVector, GcdFreeBasis, GreatestFactorialFactorization, Homogenize,
Hurwitz, IsHomogeneous, IsSelfReciprocal, MinimalPolynomial, PDEToPolynomial,
PolynomialToPDE, ShiftEquivalent, ShiftlessDecomposition, Shorten, Shorter, Sort, Split,
Splits, SquareFreePart, Translate]

#--

\# Parameters to set. n1, n2, n3 represents the vibrational energy levels for each mode.
\# Set maximum n1 (n1max), maximum n2 (n2max), maximum n3 (n3max).
$n1max := 3; n2max := 0; n3max := 0$

$$n1max := 3$$
$$n2max := 0$$
$$n3max := 0 \qquad \textbf{(3)}$$

$n1 := [seq(seq(seq(n1, n1 = 0..n1max), n2 = 0..n2max), n3 = 0..n3max)]$
$$n1 := [0, 1, 2, 3] \qquad \textbf{(4)}$$

$n2 := [seq(seq(seq(n2, n1 = 0..n1max), n2 = 0..n2max), n3 = 0..n3max)]$
$$n2 := [0, 0, 0, 0] \qquad \textbf{(5)}$$

$n3 := [seq(seq(seq(n3, n1 = 0..n1max), n2 = 0..n2max), n3 = 0..n3max)]$
$$n3 := [0, 0, 0, 0] \qquad \textbf{(6)}$$

\# number of points (nops) here represents the size of each side of the matrix
$n1size := nops(n1); n2size := nops(n2); n3size := nops(n3);$
$$n1size := 4$$
$$n2size := 4$$
$$n3size := 4 \qquad \textbf{(7)}$$

\#size $:= nops([\%])$

$size := n1size$
$$size := 4 \qquad \textbf{(8)}$$

#--

\# Define the results of the integral $<v1|q^n|v2>$, where q is defined using ladder operators.
\# q0 is $<v1|q^0|v2>$, q1 is $<v1|q^1|v2>$, ... Define q0, q1, q2, q3, q4.

$q0 := (n1, n2) \rightarrow$ **if** $n1 = n2$ **then** 1 **else** 0 **fi**
$$q0 := (n1, n2) \mapsto \textbf{if } n1 = n2 \textbf{ then } 1 \textbf{ else } 0 \textbf{ end if} \qquad \textbf{(9)}$$

$q1 := (n1, n2) \rightarrow$ **if** $n1 < 0$ **then** 0 **elif** $n2 < 0$ **then** 0 **elif** $\text{abs}(n1 - n2) = 1$ **then** $\text{sqrt}\left(\dfrac{\max(n1, n2)}{2}\right)$
else 0 **fi**

$q1 := (n1, n2) \mapsto$ **if** $n1 < 0$ **then** 0 **elif** $n2 < 0$ **then** 0 **elif** $|n1 - n2| = 1$ **then** $\sqrt{\dfrac{\max(n1, n2)}{2}}$ **(10)**
else 0 **end if**

$q2 := (n1, n2) \rightarrow add(q1(n1, i) \cdot q1(i, n2), i = n2 - 1 .. n2 + 1)$
$\qquad q2 := (n1, n2) \mapsto add(q1(n1, i)\, q1(i, n2), i = n2 - 1 .. n2 + 1)$ **(11)**

$q3 := (n1, n2) \rightarrow add(q2(n1, i) \cdot q1(i, n2), i = n2 - 1 .. n2 + 1)$
$\qquad q3 := (n1, n2) \mapsto add(q2(n1, i)\, q1(i, n2), i = n2 - 1 .. n2 + 1)$ **(12)**

$q4 := (n1, n2) \rightarrow add(q3(n1, i) \cdot q1(i, n2), i = n2 - 1 .. n2 + 1)$
$\qquad q4 := (n1, n2) \mapsto add(q3(n1, i)\, q1(i, n2), i = n2 - 1 .. n2 + 1)$ **(13)**

$q5 := (n1, n2) \rightarrow add(q4(n1, i) \cdot q1(i, n2), i = n2 - 1 .. n2 + 1)$
$\qquad q5 := (n1, n2) \mapsto add(q4(n1, i)\, q1(i, n2), i = n2 - 1 .. n2 + 1)$ **(14)**

$q6 := (n1, n2) \rightarrow add(q5(n1, i) \cdot q1(i, n2), i = n2 - 1 .. n2 + 1)$
$\qquad q6 := (n1, n2) \mapsto add(q5(n1, i)\, q1(i, n2), i = n2 - 1 .. n2 + 1)$ **(15)**

--

List the dipole moments x and y vectors for each mode.

these are the x values; x=normal mode
$xpts :=$
  $readdata(\text{"C:/Users/Kirano/Documents/Research/TheoriesAndBasisSets/ccsd(t)}$
  $/aug{-}cc{-}pvqz/InternalCoordinates/q1/DM{-}vs{-}q/q{-}range.txt", 1)$
$xpts := [-5.0, -4.5, -4.0, -3.5, -3.0, -2.5, -2.0, -1.5, -1.0, -0.5, 0., 0.5, 1.0, 1.5, 2.0,$ **(16)**
  $2.5, 3.0, 3.5, 4.0, 4.5, 5.0]$

$nops(xpts);$

$\qquad\qquad\qquad\qquad\qquad 21$ **(17)**

#Digits $:= 13$

these are the y values; y=Dipole Vector
$ypts\_DMx\_v1 :=$
  $readdata(\text{"C:/Users/Kirano/Documents/Research/TheoriesAndBasisSets/ccsd(t)/aug-cc-}$
  $pvqz/InternalCoordinates/q1/DM{-}vs{-}q/DMx.txt", 1)$
$ypts\_DMx\_v1 := [-0.2245000000, -0.2464500000, -0.2662500000, -0.2841250000,$ **(18)**
  $-0.3002250000, -0.3146000000, -0.3272500000, -0.3380750000, -0.3470000000,$
  $-0.3536750000, -0.3577250000, -0.3585000000, -0.3552250000, -0.3467500000,$
  $-0.3316000000, -0.3079250000, -0.2733250000, -0.2251250000, -0.1604750000,$

$-0.0770250000, 0.0261000000]$

$ypts\_DMy\_v1 :=$
    $readdata($"C:/Users/Kirano/Documents/Research/TheoriesAndBasisSets/ccsd(t)/aug-cc-pvqz/InternalCoordinates/q1/DM−vs−q/DMy.txt", 1$)$
$ypts\_DMy\_v1 := [0.5387750000, 0.5433250000, 0.5487000000, 0.5544000000, 0.5600000000,$ **(19)**
    $0.5649500000, 0.5687750000, 0.5709000000, 0.5707500000, 0.5675500000, 0.5606250000,$
    $0.5491250000, 0.5321250000, 0.5086000000, 0.4775000000, 0.4376000000, 0.3877500000,$
    $0.3268750000, 0.2543750000, 0.1707000000, 0.0778250000]$

$ypts\_DMx\_v2 :=$
    $readdata($"C:/Users/Kirano/Documents/Research/TheoriesAndBasisSets/ccsd(t)/aug-cc-pvqz/InternalCoordinates/q2/DM−vs−q/DMx.txt", 1$)$
$ypts\_DMx\_v2 := [0.0849750000, 0.0254000000, -0.0298500000, -0.0811000000,$ **(20)**
    $-0.1287750000, -0.1732000000, -0.2147500000, -0.2537250000, -0.2904000000,$
    $-0.3250000000, -0.3577250000, -0.3887250000, -0.4181500000, -0.4461750000,$
    $-0.4729000000, -0.4984250000, -0.5229000000, -0.5464500000, -0.5692000000,$
    $-0.5913000000, -0.6128750000]$

$ypts\_DMy\_v2 :=$
    $readdata($"C:/Users/Kirano/Documents/Research/TheoriesAndBasisSets/ccsd(t)/aug-cc-pvqz/InternalCoordinates/q2/DM−vs−q/DMy.txt", 1$)$
$ypts\_DMy\_v2 := [0.2415250000, 0.3049750000, 0.3572250000, 0.4005500000, 0.4366500000,$ **(21)**
    $0.4669500000, 0.4924500000, 0.5140500000, 0.5323000000, 0.5477000000, 0.5606250000,$
    $0.5713250000, 0.5800250000, 0.5869000000, 0.5921000000, 0.5956500000, 0.5976750000,$
    $0.5982250000, 0.5973750000, 0.5951500000, 0.5915500000]$

$ypts\_DMx\_v3 :=$
    $readdata($"C:/Users/Kirano/Documents/Research/TheoriesAndBasisSets/ccsd(t)/aug-cc-pvqz/InternalCoordinates/q3/DM−vs−q/DMx.txt", 1$)$
$ypts\_DMx\_v3 := [-0.3196250000, -0.3396750000, -0.3569000000, -0.3711000000,$ **(22)**
    $-0.3820000000, -0.3892500000, -0.3924250000, -0.3911500000, -0.3851000000,$
    $-0.3740000000, -0.3577250000, -0.3362750000, -0.3099750000, -0.2793750000,$
    $-0.2452500000, -0.2087750000, -0.1710750000, -0.1335250000, -0.0972500000,$
    $-0.0633250000, -0.0325750000]$

$ypts\_DMy\_v3 :=$
    $readdata($"C:/Users/Kirano/Documents/Research/TheoriesAndBasisSets/ccsd(t)/aug-cc-pvqz/InternalCoordinates/q3/DM−vs−q/DMy.txt", 1$)$
$ypts\_DMy\_v3 := [0.5566250000, 0.5741500000, 0.5888500000, 0.6007000000, 0.6094250000,$ **(23)**
    $0.6145000000, 0.6152750000, 0.6109750000, 0.6009000000, 0.5842750000, 0.5606250000,$
    $0.5296500000, 0.4914500000, 0.4466250000, 0.3962000000, 0.3416750000, 0.2848500000,$
    $0.2277250000, 0.1721500000, 0.1198500000, 0.0721250000]$

Identify x and y dipole moment when q=0
The x-dipole moment at q=0 will be the same for all modes, and the y-dipole moment at q=0 will be
    the same for all modes.

92

$$xDM\_no\_q := ypts\_DMx\_v1\left[\frac{(nops(xpts) + 1)}{2}\right]$$

$$xDM\_no\_q := -0.3577250000 \qquad (24)$$

$$yDM\_no\_q := ypts\_DMy\_v1\left[\frac{(nops(xpts) + 1)}{2}\right]$$

$$yDM\_no\_q := 0.5606250000 \qquad (25)$$

Give the ANHARMONIC frequencies (in cm-1) of the three modes
$v1\_anharm\_freq := 1541.83265367378$; $v2\_anharm\_freq := 1589.51100047163$; $v3\_anharm\_freq :=$
    2857.89762078017

$$v1\_anharm\_freq := 1541.83265367378$$
$$v2\_anharm\_freq := 1589.51100047163$$
$$v3\_anharm\_freq := 2857.89762078017 \qquad (26)$$

$$v1\_xDM\_Eqn := xDM\_no\_q + b\cdot x + c\cdot x^2 + d\cdot x^3 + e\cdot x^4 + f\cdot x^5$$
$$v1\_xDM\_Eqn := f x^5 + e x^4 + d x^3 + c x^2 + b x - 0.3577250000 \qquad (27)$$

recalculate the fit
$v1\_xDM\_Func := rhs(fit[leastsquare[[x, y], y = v1\_xDM\_Eqn]]([xpts, ypts\_DMx\_v1]));$
$v1\_xDM\_Func := 6.353149572\ 10^{-6}\ x^5 + 0.0001527055762\ x^4 + 0.001065994493\ x^3 \qquad (28)$
$\quad + 0.006548132126\ x^2 - 0.005497866374\ x - 0.3577250000$

$printf("xDM\_no\_q, b, c, d, e , f are:") : const\_v1\_xDM := CoefficientList(v1\_xDM\_Func, x)$
```
xDM_no_q, b, c, d, e , f are:
```
$const\_v1\_xDM := [-0.3577250000, -0.005497866374, 0.006548132126, 0.001065994493, \qquad (29)$
$\quad 0.0001527055762, 6.353149572\ 10^{-6}]$

$$k\_v1\_x\_q0 := const\_v1\_xDM_1$$
$$k\_v1\_x\_q0 := -0.3577250000 \qquad (30)$$
$$k\_v1\_x\_q1 := const\_v1\_xDM_2$$
$$k\_v1\_x\_q1 := -0.005497866374 \qquad (31)$$
$$k\_v1\_x\_q2 := const\_v1\_xDM_3$$
$$k\_v1\_x\_q2 := 0.006548132126 \qquad (32)$$
$$k\_v1\_x\_q3 := const\_v1\_xDM_4$$
$$k\_v1\_x\_q3 := 0.001065994493 \qquad (33)$$
$$k\_v1\_x\_q4 := const\_v1\_xDM_5$$
$$k\_v1\_x\_q4 := 0.0001527055762 \qquad (34)$$
$$k\_v1\_x\_q5 := const\_v1\_xDM_6$$

$$k\_v1\_x\_q5 := 6.353149572 \ 10^{-6} \tag{35}$$

--

$v1\_yDM\_Eqn := yDM\_no\_q + b \cdot x + c \cdot x^2 + d \cdot x^3 + e \cdot x^4 + f \cdot x^5$
$$v1\_yDM\_Eqn := f x^5 + e x^4 + d x^3 + c x^2 + b x + 0.5606250000 \tag{36}$$

recalculate the fit
$v1\_yDM\_Func := rhs(\,fit[\,leastsquare[\,[x, y], y = v1\_yDM\_Eqn\,]]([xpts, ypts\_DMy\_v1]));$
$$v1\_yDM\_Func := 5.728256497 \ 10^{-6} x^5 - 0.00002737681533 \ x^4 - 0.001278042438 \ x^3 \tag{37}$$
$$- \ 0.009447662847 \ x^2 - 0.01777263229 \ x + 0.5606250000$$

$printf(\text{"yDM\_no\_q, b, c, d, e, f are:"}) : const\_v1\_yDM := CoefficientList(v1\_yDM\_Func, x)$
yDM_no_q, b, c, d, e, f are:
$$const\_v1\_yDM := [0.5606250000, -0.01777263229, -0.009447662847, -0.001278042438, \tag{38}$$
$$-0.00002737681533, 5.728256497 \ 10^{-6}]$$

$k\_v1\_y\_q0 := const\_v1\_yDM_1$
$$k\_v1\_y\_q0 := 0.5606250000 \tag{39}$$
$k\_v1\_y\_q1 := const\_v1\_yDM_2$
$$k\_v1\_y\_q1 := -0.01777263229 \tag{40}$$
$k\_v1\_y\_q2 := const\_v1\_yDM_3$
$$k\_v1\_y\_q2 := -0.009447662847 \tag{41}$$
$k\_v1\_y\_q3 := const\_v1\_yDM_4$
$$k\_v1\_y\_q3 := -0.001278042438 \tag{42}$$
$k\_v1\_y\_q4 := const\_v1\_yDM_5$
$$k\_v1\_y\_q4 := -0.00002737681533 \tag{43}$$
$k\_v1\_y\_q5 := const\_v1\_yDM_6$
$$k\_v1\_y\_q5 := 5.728256497 \ 10^{-6} \tag{44}$$

--

$v2\_xDM\_Eqn := xDM\_no\_q + b \cdot x + c \cdot x^2 + d \cdot x^3 + e \cdot x^4 + f \cdot x^5$
$$v2\_xDM\_Eqn := f x^5 + e x^4 + d x^3 + c x^2 + b x - 0.3577250000 \tag{45}$$

recalculate the fit
$v2\_xDM\_Func := rhs(\,fit[\,leastsquare[\,[x, y], y = v2\_xDM\_Eqn\,]]([xpts, ypts\_DMx\_v2]));$
$$v2\_xDM\_Func := -1.102557915 \ 10^{-6} x^5 + 0.00001292633055 \ x^4 - 0.0002182779573 \ x^3 \tag{46}$$
$$+ \ 0.003429057780 \ x^2 - 0.06364249220 \ x - 0.3577250000$$

$printf(\text{"xDM\_no\_q, b, c, d, e, f are:"}) : const\_v2\_xDM := CoefficientList(v2\_xDM\_Func, x)$
xDM_no_q, b, c, d, e, f are:
$$const\_v2\_xDM := [-0.3577250000, -0.06364249220, 0.003429057780, -0.0002182779573, \tag{47}$$

94

$$0.00001292633055, -1.102557915 \ 10^{-6}]$$

$k\_v2\_x\_q0 := const\_v2\_xDM_1$

$$k\_v2\_x\_q0 := -0.3577250000 \tag{48}$$

$k\_v2\_x\_q1 := const\_v2\_xDM_2$

$$k\_v2\_x\_q1 := -0.06364249220 \tag{49}$$

$k\_v2\_x\_q2 := const\_v2\_xDM_3$

$$k\_v2\_x\_q2 := 0.003429057780 \tag{50}$$

$k\_v2\_x\_q3 := const\_v2\_xDM_4$

$$k\_v2\_x\_q3 := -0.0002182779573 \tag{51}$$

$k\_v2\_x\_q4 := const\_v2\_xDM_5$

$$k\_v2\_x\_q4 := 0.00001292633055 \tag{52}$$

$k\_v2\_x\_q5 := const\_v2\_xDM_6$

$$k\_v2\_x\_q5 := -1.102557915 \ 10^{-6} \tag{53}$$

--

$v2\_yDM\_Eqn := yDM\_no\_q + b \cdot x + c \cdot x^2 + d \cdot x^3 + e \cdot x^4 + f \cdot x^5$
$$v2\_yDM\_Eqn := f x^5 + e x^4 + d x^3 + c x^2 + b x + 0.5606250000 \tag{54}$$

recalculate the fit
$v2\_yDM\_Func := rhs(fit[leastsquare[[x, y], y = v2\_yDM\_Eqn]]([xpts, ypts\_DMy\_v2]));$
$$v2\_yDM\_Func := 6.026897780 \ 10^{-6} x^5 - 0.00005854774208 \ x^4 + 0.0003058144811 \ x^3 \tag{55}$$
$$- 0.004288476042 \ x^2 + 0.02358596791 \ x + 0.5606250000$$

$printf("yDM\_no\_q, b, c, d, e , f \ are:") : const\_v2\_yDM := CoefficientList(v2\_yDM\_Func, x)$
yDM_no_q, b, c, d, e , f are:
$$const\_v2\_yDM := [0.5606250000, 0.02358596791, -0.004288476042, 0.0003058144811, \tag{56}$$
$$-0.00005854774208, 6.026897780 \ 10^{-6}]$$

$k\_v2\_y\_q0 := const\_v2\_yDM_1$

$$k\_v2\_y\_q0 := 0.5606250000 \tag{57}$$

$k\_v2\_y\_q1 := const\_v2\_yDM_2$

$$k\_v2\_y\_q1 := 0.02358596791 \tag{58}$$

$k\_v2\_y\_q2 := const\_v2\_yDM_3$

$$k\_v2\_y\_q2 := -0.004288476042 \tag{59}$$

$k\_v2\_y\_q3 := const\_v2\_yDM_4$

$$k\_v2\_y\_q3 := 0.0003058144811 \tag{60}$$

$k\_v2\_y\_q4 := const\_v2\_yDM_5$

$$k\_v2\_y\_q4 := -0.00005854774208 \tag{61}$$

$k\_v2\_y\_q5 := const\_v2\_yDM_6$

$$k\_v2\_y\_q5 := 6.026897780 \ 10^{-6} \tag{62}$$

95

$v3\_xDM\_Eqn := xDM\_no\_q + b \cdot x + c \cdot x^2 + d \cdot x^3 + e \cdot x^4 + f \cdot x^5$

$$v3\_xDM\_Eqn := f x^5 + e x^4 + d x^3 + c x^2 + b x - 0.3577250000 \tag{63}$$

recalculate the fit
$v3\_xDM\_Func := rhs(\, fit[\,leastsquare[\,[x, y], y = v3\_xDM\_Eqn\,]]([\,xpts, ypts\_DMx\_v3\,])\,);$

$$v3\_xDM\_Func := -2.988556797\ 10^{-6} x^5 - 0.0001093197246\ x^4 - 0.0002993556753\ x^3 \tag{64}$$
$$+ 0.009966323469\ x^2 + 0.03803436445\ x - 0.3577250000$$

$printf(\text{"xDM\_no\_q, b, c, d, e , f are:"}) : const\_v3\_xDM := CoefficientList(v3\_xDM\_Func, x)$
```
xDM_no_q, b, c, d, e , f are:
```
$$const\_v3\_xDM := [\,-0.3577250000, 0.03803436445, 0.009966323469, -0.0002993556753, \tag{65}$$
$$-0.0001093197246, -2.988556797\ 10^{-6}\,]$$

$k\_v3\_x\_q0 := const\_v3\_xDM_1$

$$k\_v3\_x\_q0 := -0.3577250000 \tag{66}$$

$k\_v3\_x\_q1 := const\_v3\_xDM_2$

$$k\_v3\_x\_q1 := 0.03803436445 \tag{67}$$

$k\_v3\_x\_q2 := const\_v3\_xDM_3$

$$k\_v3\_x\_q2 := 0.009966323469 \tag{68}$$

$k\_v3\_x\_q3 := const\_v3\_xDM_4$

$$k\_v3\_x\_q3 := -0.0002993556753 \tag{69}$$

$k\_v3\_x\_q4 := const\_v3\_xDM_5$

$$k\_v3\_x\_q4 := -0.0001093197246 \tag{70}$$

$k\_v3\_x\_q5 := const\_v3\_xDM_6$

$$k\_v3\_x\_q5 := -2.988556797\ 10^{-6} \tag{71}$$

$v3\_yDM\_Eqn := yDM\_no\_q + b \cdot x + c \cdot x^2 + d \cdot x^3 + e \cdot x^4 + f \cdot x^5$

$$v3\_yDM\_Eqn := f x^5 + e x^4 + d x^3 + c x^2 + b x + 0.5606250000 \tag{72}$$

recalculate the fit
$v3\_yDM\_Func := rhs(\, fit[\,leastsquare[\,[x, y], y = v3\_yDM\_Eqn\,]]([\,xpts, ypts\_DMy\_v3\,])\,);$

$$v3\_yDM\_Func := 9.199317679\ 10^{-6} x^5 + 0.0001718271804\ x^4 + 0.00003630441029\ x^3 \tag{73}$$
$$- 0.01409266917\ x^2 - 0.05506493094\ x + 0.5606250000$$

$printf(\text{"yDM\_no\_q, b, c, d, e , f are:"}) : const\_v3\_yDM := CoefficientList(v3\_yDM\_Func, x)$
```
yDM_no_q, b, c, d, e , f are:
```
$$const\_v3\_yDM := [\,0.5606250000, -0.05506493094, -0.01409266917, 0.00003630441029, \tag{74}$$
$$0.0001718271804, 9.199317679\ 10^{-6}\,]$$

$k\_v3\_y\_q0 := const\_v3\_yDM_1$

$$k\_v3\_y\_q0 := 0.5606250000 \qquad (75)$$

$k\_v3\_y\_q1 := const\_v3\_yDM_2$

$$k\_v3\_y\_q1 := -0.05506493094 \qquad (76)$$

$k\_v3\_y\_q2 := const\_v3\_yDM_3$

$$k\_v3\_y\_q2 := -0.01409266917 \qquad (77)$$

$k\_v3\_y\_q3 := const\_v3\_yDM_4$

$$k\_v3\_y\_q3 := 0.00003630441029 \qquad (78)$$

$k\_v3\_y\_q4 := const\_v3\_yDM_5$

$$k\_v3\_y\_q4 := 0.0001718271804 \qquad (79)$$

$k\_v3\_y\_q5 := const\_v3\_yDM_6$

$$k\_v3\_y\_q5 := 9.199317679 \ 10^{-6} \qquad (80)$$

\# ---

\# List all of the eigenvectors from lowest Energy level (lowest eigenvalue) <-list "Eigvect_v0", and list all of the eigenvectors from the next lowest Energy level (second lowest eigenvalue) <-list "Eigvect_v1".

\# The mode that each eigenvector describes will be in title --> ex. eigenvectors that describe lowest energy level for normal mode 1 is titled "Eigvect_v0_mode1"

\# For mode 1:

$Eigvect\_state0\_v1 :=$
$$\begin{bmatrix} 0.9998658167623 & -0.01583004563139 & 0.0001020009946264 & -0.004212804580395 \end{bmatrix}:$$
$Eigvect\_state0\_v1 := Matrix(Eigvect\_state0\_v1)$

$Eigvect\_state0\_v1 := \qquad (81)$
$$[\,0.9998658167623, \ -0.01583004563139, \ 0.0001020009946264,$$
$$-0.004212804580395\,]$$

$Eigvect\_state1\_v1 := \langle 0.01582213462534, 0.9988943860429, -0.04426256023948,$
$0.0007009639895876 \rangle : Eigvect\_state1\_v1 := Matrix(Eigvect\_state1\_v1)$

$$Eigvect\_state1\_v1 := \begin{bmatrix} 0.01582213462534 \\ 0.9988943860429 \\ -0.04426256023948 \\ 0.0007009639895876 \end{bmatrix} \qquad (82)$$

\# For mode 2

$Eigvect\_state0\_v2 :=$
$$\begin{bmatrix} 0.9988101763001 & 0.04700728260698 & 0.002570087188967 & 0.01272563367080 \end{bmatrix}:$$
$Eigvect\_state0\_v2 := Matrix(Eigvect\_state0\_v2)$

Eigvect_state0_v2 := (83)

$$\begin{bmatrix} 0.9988101763001 & 0.04700728260698 & 0.002570087188967 & 0.01272563367080 \end{bmatrix}$$

Eigvect_state1_v2 := ⟨−0.04705385068098, 0.9901803313392, 0.1313304274160, 0.009009184159322⟩ : *Eigvect_state1_v2* := *Matrix(Eigvect_state1_v2)*

$$Eigvect\_state1\_v2 := \begin{bmatrix} -0.04705385068098 \\ 0.9901803313392 \\ 0.1313304274160 \\ 0.009009184159322 \end{bmatrix}$$ (84)

For mode 3

Eigvect_state0_v3 :=
$$\begin{bmatrix} 0.9913061684432 & 0.1263834757661 & 0.01473639167681 & 0.03349830174750 \end{bmatrix} :$$
Eigvect_state0_v3 := *Matrix(Eigvect_state0_v3)*

Eigvect_state0_v3 := (85)

$$\begin{bmatrix} 0.9913061684432 & 0.1263834757661 & 0.01473639167681 & 0.03349830174750 \end{bmatrix}$$

Eigvect_state1_v3 := ⟨−0.1255163020413, 0.9323459414381, 0.3354943228465, 0.04919616595636⟩ : *Eigvect_state1_v3* := *Matrix(Eigvect_state1_v3)*

$$Eigvect\_state1\_v3 := \begin{bmatrix} -0.1255163020413 \\ 0.9323459414381 \\ 0.3354943228465 \\ 0.04919616595636 \end{bmatrix}$$ (86)

#--

0 --> = $q1^0 q2^0 q3^0$
$mat0 := matrix(size, size, [seq(seq(q0(n1[r], n1[c]) \cdot q0(n2[r], n2[c]) \cdot q0(n3[r], n3[c]), c = 1\ ..size), r = 1\ ..size)])$

$$mat0 := \begin{bmatrix} 1 & 0 & 0 & 0 \\ 0 & 1 & 0 & 0 \\ 0 & 0 & 1 & 0 \\ 0 & 0 & 0 & 1 \end{bmatrix}$$ (87)

1 --> = $q1^1 q2^0 q3^0$
$mat1 := matrix(size, size, [seq(seq(q1(n1[r], n1[c]) \cdot q0(n2[r], n2[c]) \cdot q0(n3[r], n3[c]), c = 1\ ..size), r = 1\ ..size)])$

$$mat1 := \begin{bmatrix} 0 & \dfrac{\sqrt{2}}{2} & 0 & 0 \\[2mm] \dfrac{\sqrt{2}}{2} & 0 & 1 & 0 \\[2mm] 0 & 1 & 0 & \dfrac{\sqrt{6}}{2} \\[2mm] 0 & 0 & \dfrac{\sqrt{6}}{2} & 0 \end{bmatrix} \qquad (88)$$

2 --> $= q1^0 q2^1 q3^0$
$mat2 := matrix(size, size, [seq(seq(q0(n1[r], n1[c]) \cdot q1(n2[r], n2[c]) \cdot q0(n3[r], n3[c]), c = 1 ..size), r = 1 ..size)])$

$$mat2 := \begin{bmatrix} 0 & 0 & 0 & 0 \\ 0 & 0 & 0 & 0 \\ 0 & 0 & 0 & 0 \\ 0 & 0 & 0 & 0 \end{bmatrix} \qquad (89)$$

3 --> $= q1^0 q2^0 q3^1$
$mat3 := matrix(size, size, [seq(seq(q0(n1[r], n1[c]) \cdot q0(n2[r], n2[c]) \cdot q1(n3[r], n3[c]), c = 1 ..size), r = 1 ..size)])$

$$mat3 := \begin{bmatrix} 0 & 0 & 0 & 0 \\ 0 & 0 & 0 & 0 \\ 0 & 0 & 0 & 0 \\ 0 & 0 & 0 & 0 \end{bmatrix} \qquad (90)$$

11 --> $= q1^2 q2^0 q3^0$
$mat11 := matrix(size, size, [seq(seq(q2(n1[r], n1[c]) \cdot q0(n2[r], n2[c]) \cdot q0(n3[r], n3[c]), c = 1 ..size), r = 1 ..size)])$

$$mat11 := \begin{bmatrix} \dfrac{1}{2} & 0 & \dfrac{\sqrt{2}}{2} & 0 \\[2mm] 0 & \dfrac{3}{2} & 0 & \dfrac{\sqrt{6}}{2} \\[2mm] \dfrac{\sqrt{2}}{2} & 0 & \dfrac{5}{2} & 0 \\[2mm] 0 & \dfrac{\sqrt{6}}{2} & 0 & \dfrac{7}{2} \end{bmatrix} \qquad (91)$$

22 --> $= q1^0 q2^2 q3^0$

$mat22 := matrix(size, size, [seq(seq(q0(n1[r], n1[c]) \cdot q2(n2[r], n2[c]) \cdot q0(n3[r], n3[c]), c=1$
$..size), r=1..size)])$

$$mat22 := \begin{bmatrix} \frac{1}{2} & 0 & 0 & 0 \\ 0 & \frac{1}{2} & 0 & 0 \\ 0 & 0 & \frac{1}{2} & 0 \\ 0 & 0 & 0 & \frac{1}{2} \end{bmatrix} \tag{92}$$

33 --> $= q1^0 q2^0 q3^2$
$mat33 := matrix(size, size, [seq(seq(q0(n1[r], n1[c]) \cdot q0(n2[r], n2[c]) \cdot q2(n3[r], n3[c]), c=1$
$..size), r=1..size)])$

$$mat33 := \begin{bmatrix} \frac{1}{2} & 0 & 0 & 0 \\ 0 & \frac{1}{2} & 0 & 0 \\ 0 & 0 & \frac{1}{2} & 0 \\ 0 & 0 & 0 & \frac{1}{2} \end{bmatrix} \tag{93}$$

111 --> $= q1^3 q2^0 q3^0$
$mat111 := matrix(size, size, [seq(seq(q3(n1[r], n1[c]) \cdot q0(n2[r], n2[c]) \cdot q0(n3[r], n3[c]), c=1$
$..size), r=1..size)])$

$$mat111 := \begin{bmatrix} 0 & \frac{3\sqrt{2}}{4} & 0 & \frac{\sqrt{2}\sqrt{6}}{4} \\ \frac{3\sqrt{2}}{4} & 0 & 3 & 0 \\ 0 & 3 & 0 & \frac{9\sqrt{6}}{4} \\ \frac{\sqrt{2}\sqrt{6}}{4} & 0 & \frac{9\sqrt{6}}{4} & 0 \end{bmatrix} \tag{94}$$

222 --> $= q1^0 q2^3 q3^0$
$mat222 := matrix(size, size, [seq(seq(q0(n1[r], n1[c]) \cdot q3(n2[r], n2[c]) \cdot q0(n3[r], n3[c]), c=1$
$..size), r=1..size)])$

$$mat222 := \begin{bmatrix} 0 & 0 & 0 & 0 \\ 0 & 0 & 0 & 0 \\ 0 & 0 & 0 & 0 \\ 0 & 0 & 0 & 0 \end{bmatrix} \tag{95}$$

333 --> = $q1^0 q2^0 q3^3$
$mat333 := matrix(size, size, [seq(seq(q0(n1[r], n1[c]) \cdot q0(n2[r], n2[c]) \cdot q3(n3[r], n3[c]), c = 1$
$\quad ..size), r = 1 ..size)])$

$$mat333 := \begin{bmatrix} 0 & 0 & 0 & 0 \\ 0 & 0 & 0 & 0 \\ 0 & 0 & 0 & 0 \\ 0 & 0 & 0 & 0 \end{bmatrix} \tag{96}$$

1111 --> = $q1^4 q2^0 q3^0$
$mat1111 := matrix(size, size, [seq(seq(q4(n1[r], n1[c]) \cdot q0(n2[r], n2[c]) \cdot q0(n3[r], n3[c]), c = 1$
$\quad ..size), r = 1 ..size)])$

$$mat1111 := \begin{bmatrix} \dfrac{3}{4} & 0 & \dfrac{3\sqrt{2}}{2} & 0 \\ 0 & \dfrac{15}{4} & 0 & \dfrac{5\sqrt{6}}{2} \\ \dfrac{3\sqrt{2}}{2} & 0 & \dfrac{39}{4} & 0 \\ 0 & \dfrac{5\sqrt{6}}{2} & 0 & \dfrac{75}{4} \end{bmatrix} \tag{97}$$

2222 --> = $q1^0 q2^4 q3^0$
$mat2222 := matrix(size, size, [seq(seq(q0(n1[r], n1[c]) \cdot q4(n2[r], n2[c]) \cdot q0(n3[r], n3[c]), c = 1$
$\quad ..size), r = 1 ..size)])$

$$mat2222 := \begin{bmatrix} \dfrac{3}{4} & 0 & 0 & 0 \\ 0 & \dfrac{3}{4} & 0 & 0 \\ 0 & 0 & \dfrac{3}{4} & 0 \\ 0 & 0 & 0 & \dfrac{3}{4} \end{bmatrix} \tag{98}$$

3333 --> = $q1^0 q2^0 q3^4$
$mat3333 := matrix(size, size, [seq(seq(q0(n1[r], n1[c]) \cdot q0(n2[r], n2[c]) \cdot q4(n3[r], n3[c]), c = 1$
$\quad ..size), r = 1 ..size)])$

101

$$mat3333 := \begin{bmatrix} \dfrac{3}{4} & 0 & 0 & 0 \\[2mm] 0 & \dfrac{3}{4} & 0 & 0 \\[2mm] 0 & 0 & \dfrac{3}{4} & 0 \\[2mm] 0 & 0 & 0 & \dfrac{3}{4} \end{bmatrix} \tag{99}$$

11111 --> = $q1^5 q2^0 q3^0$
$mat11111 := matrix(size, size, [seq(seq(q5(n1[r], n1[c]) \cdot q0(n2[r], n2[c]) \cdot q0(n3[r], n3[c]), c=1$
..$size), r=1 ..size)])$

$$mat11111 := \begin{bmatrix} 0 & \dfrac{15\sqrt{2}}{8} & 0 & \dfrac{5\sqrt{2}\,\sqrt{6}}{4} \\[3mm] \dfrac{15\sqrt{2}}{8} & 0 & \dfrac{45}{4} & 0 \\[3mm] 0 & \dfrac{45}{4} & 0 & \dfrac{95\sqrt{6}}{8} \\[3mm] \dfrac{5\sqrt{2}\,\sqrt{6}}{4} & 0 & \dfrac{95\sqrt{6}}{8} & 0 \end{bmatrix} \tag{100}$$

22222 --> = $q1^0 q2^5 q3^0$
$mat22222 := matrix(size, size, [seq(seq(q0(n1[r], n1[c]) \cdot q5(n2[r], n2[c]) \cdot q0(n3[r], n3[c]), c=1$
..$size), r=1 ..size)])$

$$mat22222 := \begin{bmatrix} 0 & 0 & 0 & 0 \\ 0 & 0 & 0 & 0 \\ 0 & 0 & 0 & 0 \\ 0 & 0 & 0 & 0 \end{bmatrix} \tag{101}$$

33333 --> = $q1^0 q2^0 q3^5$
$mat33333 := matrix(size, size, [seq(seq(q0(n1[r], n1[c]) \cdot q0(n2[r], n2[c]) \cdot q5(n3[r], n3[c]), c=1$
..$size), r=1 ..size)])$

$$mat33333 := \begin{bmatrix} 0 & 0 & 0 & 0 \\ 0 & 0 & 0 & 0 \\ 0 & 0 & 0 & 0 \\ 0 & 0 & 0 & 0 \end{bmatrix} \tag{102}$$

--

Calculating transition dipole moment of q1

102

#---- *Calculating the x—vector transition dipole moment:*

$mat\_sum\_v1\_x := evalm(k\_v1\_x\_q0 \cdot mat0 + k\_v1\_x\_q1 \cdot mat1 + k\_v1\_x\_q2 \cdot mat11 + k\_v1\_x\_q3$
$\quad \cdot mat111 + k\_v1\_x\_q4 \cdot mat1111 + k\_v1\_x\_q5 \cdot mat11111)$

$mat\_sum\_v1\_x := \big[\big[-0.3543364047, \ -0.001937525162\sqrt{2}, \ 0.003503124427\sqrt{2},$ **(103)**

$\quad 0.0002744400602\sqrt{2}\sqrt{6}\,\big],$

$\quad \big[-0.001937525162\sqrt{2}, \ -0.3473301559, \ -0.002228409962, \ 0.003655830004\sqrt{6}\,\big],$

$\quad \big[0.003503124427\sqrt{2}, \ -0.002228409962, \ -0.3398657903, \ -0.0002750019268\sqrt{6}\,\big],$

$\quad \big[0.0002744400602\sqrt{2}\sqrt{6}, \ 0.003655830004\sqrt{6}, \ -0.0002750019268\sqrt{6},$

$\quad -0.3319433080\,\big]\big]$

Up to the n-th derivative of dipole function at q=0 (here labeled "k_v1_x_q0" for the zeroth derivative,
"k_v1_x_q1" for the first derivative, etc.) multiplied with the integral of $\langle \varphi\_(harm, v = i)\,|\,q$
$^n\,|\,\varphi\_(harm, v = j)\rangle$.

$dipintegral\_v1\_x := evalf(evalm(mat\_sum\_v1\_x))$

$dipintegral\_v1\_x :=$ **(104)**

$$\begin{bmatrix} -0.3543364047 & -0.002740074361 & 0.004954166074 & 0.0009506882558 \\ -0.002740074361 & -0.3473301559 & -0.002228409962 & 0.008954918097 \\ 0.004954166074 & -0.002228409962 & -0.3398657903 & -0.0006736143990 \\ 0.0009506882558 & 0.008954918097 & -0.0006736143990 & -0.3319433080 \end{bmatrix}$$

Make a matrix of the product of the eigenvectors of the lowest energy and the next lowest energy
$coeffprod\_v1 := Eigvect\_state1\_v1 \cdot Eigvect\_state0\_v1$

$coeffprod\_v1 := \big[\big[0.0158200115600886, \ -0.000250465113105128,$ **(105)**

$\quad 1.61387346889748\ 10^{-6}, \ -0.0000666555612212587\,\big],$

$\quad \big[0.998760351160060, \ -0.0158125437119984, \ 0.000101888220903103,$

$\quad -0.00420814684485238\,\big],$

$\quad \big[-0.0442566209458382, \ 0.000700678348353117, \ -4.51482516913791\ 10^{-6},$

$\quad 0.000186469516516891\,\big],$

$\quad \big[0.000700869931969966, \ -0.0000110962919411329, \ 7.14990241352247\ 10^{-8},$

$\quad -2.95302430602659\ 10^{-6}\,\big]\big]$

Integral of anharmonic wave functions with dipole vector operator multiplied by its product of
eigenvectors, summed.
This gives the contibrution from the x-dipole vector towards the transition dipole moment.
$x\_TDM\_v1 := add(add(dipintegral\_v1\_x[i,j] \cdot coeffprod\_v1[i,j], j = 1..4), i = 1..4)$

$\qquad\qquad x\_TDM\_v1 := -0.00310525020779377$ **(106)**

#---- *Calculating the y—vector transition dipole moment:*

$mat\_sum\_v1\_y := evalm(k\_v1\_y\_q0 \cdot mat0 + k\_v1\_y\_q1 \cdot mat1 + k\_v1\_y\_q2 \cdot mat11 + k\_v1\_y\_q3$

$\cdot mat111 + k\_v1\_y\_q4 \cdot mat1111 + k\_v1\_y\_q5 \cdot mat11111)$

$mat\_sum\_v1\_y := \left[\left[\, 0.5558806360,\ -0.009834107493\,\sqrt{2}\,,\ -0.004764896647\,\sqrt{2}\,,\right.\right.$ **(107)**

$\left. -0.0003123502889\,\sqrt{2}\,\sqrt{6}\,\right],$

$\left[\, -0.009834107493\,\sqrt{2}\,,\ 0.5463508426,\ -0.02154231671,\ -0.004792273462\,\sqrt{6}\,\right],$

$\left[\, -0.004764896647\,\sqrt{2}\,,\ -0.02154231671,\ 0.5367389190,\ -0.01169388858\,\sqrt{6}\,\right],$

$\left[\, -0.0003123502889\,\sqrt{2}\,\sqrt{6}\,,\ -0.004792273462\,\sqrt{6}\,,\ -0.01169388858\,\sqrt{6}\,,\right.$

$\left.\left. 0.5270448647\,\right]\right]$

Up to the n-th derivative of dipole function at q=0 (here labeled "k_v1_y_q0" for the zeroth derivative, "k_v1_y_q1" for the first derivative, etc.) multiplied with the integral of $\langle \varphi\_(harm, \nu = i)\,|\,q$
$\wedge n\,|\,\varphi\_(harm, \nu = j)\rangle.$

$dipintegral\_v1\_y := evalf(evalm(mat\_sum\_v1\_y))$

$dipintegral\_v1\_y :=$ **(108)**

$$\begin{bmatrix} 0.5558806360 & -0.01390752819 & -0.006738581460 & -0.001082013140 \\ -0.01390752819 & 0.5463508426 & -0.02154231671 & -0.01173862469 \\ -0.006738581460 & -0.02154231671 & 0.5367389190 & -0.02864406013 \\ -0.001082013140 & -0.01173862469 & -0.02864406013 & 0.5270448647 \end{bmatrix}$$

Make a matrix of the product of the eigenvectors of the lowest energy and the next lowest energy

$coeffprod\_v1 := Eigvect\_state1\_v1 \cdot Eigvect\_state0\_v1$

$coeffprod\_v1 := \left[\left[\, 0.0158200115600886,\ -0.000250465113105128,\right.\right.$ **(109)**

$\left. 1.61387346889748\ 10^{-6},\ -0.0000666555612212587\,\right],$

$\left[\, 0.998760351160060,\ -0.0158125437119984,\ 0.000101888220903103,\right.$

$\left. -0.00420814684485238\,\right],$

$\left[\, -0.0442566209458382,\ 0.000700678348353117,\ -4.51482516913791\ 10^{-6},\right.$

$\left. 0.000186469516516891\,\right],$

$\left[\, 0.000700869931969966,\ -0.0000110962919411329,\ 7.14990241352247\ 10^{-8},\right.$

$\left.\left. -2.95302430602659\ 10^{-6}\,\right]\right]$

Integral of anharmonic wave functions with dipole vector operator multiplied by its product of eigenvectors, summed.
This gives the contibrution from the y-dipole vector towards the transition dipole moment.

$y\_TDM\_v1 := add(add(dipintegral\_v1\_y[i,j] \cdot coeffprod\_v1[i,j], j = 1..4), i = 1..4)$

$\qquad\qquad y\_TDM\_v1 := -0.0134115171217542$ **(110)**

####Calculate the TOTAL transition dipole moment SQUARED

$Tot\_TDM\_v1\_sqr := (x\_TDM\_v1)^2 + (y\_TDM\_v1)^2$

$\qquad\qquad Tot\_TDM\_v1\_sqr := 0.000189511370360109$ **(111)**

Plug the squared total transition dipole moment into molar absorptivity equation to get the Molar Absorptivity of q1

 # Use the harmonic frequency of q1

$$MolAbs\_v1 := \frac{41.6238 \cdot \left(Tot\_TDM\_v1\_sqr \cdot (2.541765)^2 \right) \cdot v1\_anharm\_freq}{16.6054}$$

$$MolAbs\_v1 := 4.73190139569590 \tag{112}$$

 # --

Calculating transition dipole moment of q2

#---- Calculating the x−vector transition dipole moment:

$mat\_sum\_v2\_x := evalm(k\_v2\_x\_q0 \cdot mat0 + k\_v2\_x\_q1 \cdot mat2 + k\_v2\_x\_q2 \cdot mat22 + k\_v2\_x\_q3$
$\cdot mat222 + k\_v2\_x\_q4 \cdot mat2222 + k\_v2\_x\_q5 \cdot mat22222)$

$$mat\_sum\_v2\_x := \begin{bmatrix} -0.3560007764 & 0. & 0. & 0. \\ 0. & -0.3560007764 & 0. & 0. \\ 0. & 0. & -0.3560007764 & 0. \\ 0. & 0. & 0. & -0.3560007764 \end{bmatrix} \tag{113}$$

 # Up to the n-th derivative of dipole function at q=0 (here labeled "k_v2_x_q0" for the zeroth derivative,
"k_v2_x_q1" for the first derivative, etc.) multiplied with the integral of $\langle \varphi\_(harm, v=i) | q$
$^n | \varphi\_(harm, v=j) \rangle$.
$dipintegral\_v2\_x := evalf(evalm(mat\_sum\_v2\_x))$
$dipintegral\_v2\_x :=$ $\tag{114}$

$$\begin{bmatrix} -0.3560007764 & 0. & 0. & 0. \\ 0. & -0.3560007764 & 0. & 0. \\ 0. & 0. & -0.3560007764 & 0. \\ 0. & 0. & 0. & -0.3560007764 \end{bmatrix}$$

 # Make a matrix of the product of the eigenvectors of the lowest energy and the next lowest energy
$coeffprod\_v2 := Eigvect\_state1\_v2 \cdot Eigvect\_state0\_v2$
$coeffprod\_v2 := [[-0.0469978648942682, -0.00221187365670747,$ $\tag{115}$
$\quad -0.000120932498826753, -0.000598790066566675],$
$\quad [0.989002191313798, 0.0465456866671349, 0.00254484978434198,$
$\quad 0.0126006721646540],$
$\quad [0.131174167360942, 0.00617348651643939, 0.000337530649023422,$
$\quad 0.00167126290912561],$
$\quad [0.00899846481849247, 0.000423497265835577, 0.0000231543887909179,$
$\quad 0.000114647577284306]]$

 # Integral of anharmonic wave functions with dipole vector operator multiplied by its product of
eigenvectors, summed.
 # This gives the contibrution from the x-dipole vector towards the transition dipole moment.
$x\_TDM\_v2 := add(add(dipintegral\_v2\_x[i, j] \cdot coeffprod\_v2[i, j], j=1..4), i=1..4)$

$$x\_TDM\_v2 := 2.93924078327047 \; 10^{-13} \tag{116}$$

#---- Calculating the y-vector transition dipole moment:

$$mat\_sum\_v2\_y := evalm(k\_v2\_y\_q0 \cdot mat0 + k\_v2\_y\_q1 \cdot mat2 + k\_v2\_y\_q2 \cdot mat22 + k\_v2\_y\_q3 \\ \cdot mat222 + k\_v2\_y\_q4 \cdot mat2222 + k\_v2\_y\_q5 \cdot mat22222)$$

$$mat\_sum\_v2\_y := \begin{bmatrix} 0.5584368512 & 0. & 0. & 0. \\ 0. & 0.5584368512 & 0. & 0. \\ 0. & 0. & 0.5584368512 & 0. \\ 0. & 0. & 0. & 0.5584368512 \end{bmatrix} \tag{117}$$

Up to the n-th derivative of dipole function at q=0 (here labeled "k_v2_y_q0" for the zeroth derivative, "k_v2_y_q1" for the first derivative, etc.) multiplied with the integral of $\langle \varphi\_ (harm, \nu = i) | q$ ^n $| \varphi\_ (harm, \nu = j) \rangle$.

$$dipintegral\_v2\_y := evalf(evalm(mat\_sum\_v2\_y))$$

$$dipintegral\_v2\_y := \begin{bmatrix} 0.5584368512 & 0. & 0. & 0. \\ 0. & 0.5584368512 & 0. & 0. \\ 0. & 0. & 0.5584368512 & 0. \\ 0. & 0. & 0. & 0.5584368512 \end{bmatrix} \tag{118}$$

Make a matrix of the product of the eigenvectors of the lowest energy and the next lowest energy

$$coeffprod\_v2 := Eigvect\_state1\_v2 \cdot Eigvect\_state0\_v2$$

$$coeffprod\_v2 := [\, [\, -0.0469978648942682, \; -0.00221187365670747, \tag{119}$$
$$-0.000120932498826753, \; -0.000598790066566675\,],$$
$$[\, 0.989002191313798, \; 0.0465456866671349, \; 0.00254484978434198,$$
$$0.0126006721646540\,],$$
$$[\, 0.131174167360942, \; 0.00617348651643939, \; 0.000337530649023422,$$
$$0.00167126290912561\,],$$
$$[\, 0.00899846481849247, \; 0.000423497265835577, \; 0.0000231543887909179,$$
$$0.000114647577284306\,]\,]$$

Integral of anharmonic wave functions with dipole vector operator multiplied by its product of eigenvectors, summed.
This gives the contibrution from the y-dipole vector towards the transition dipole moment.

$$y\_TDM\_v2 := add(add(dipintegral\_v2\_y[i,j] \cdot coeffprod\_v2[i,j], j = 1 ..4), i = 1 ..4)$$

$$y\_TDM\_v2 := -4.61055672806854 \; 10^{-13} \tag{120}$$

Calculate the TOTAL transition dipole moment SQUARED

$$Tot\_TDM\_v2\_sqr := (x\_TDM\_v2)^2 + (y\_TDM\_v2)^2$$

$$Tot\_TDM\_v2\_sqr := 2.98963697247785 \; 10^{-25} \tag{121}$$

Plug the squared total transition dipole moment into molar absorptivity equation to get the Molar

106

Absorptivity of q2
Use the harmonic frequency of q2

$$MolAbs\_v2 := \frac{41.6238 \cdot \left(Tot\_TDM\_v2\_sqr \cdot (2.541765)^2\right) \cdot v2\_anharm\_freq}{16.6054}$$

$$MolAbs\_v2 := 7.69564753580083 \ 10^{-21} \tag{122}$$

Calculating transition dipole moment of q3

#---- *Calculating the x−vector transition dipole moment:*

$mat\_sum\_v3\_x := evalm(k\_v3\_x\_q0 \cdot mat0 + k\_v3\_x\_q1 \cdot mat3 + k\_v3\_x\_q2 \cdot mat33 + k\_v3\_x\_q3$
$\quad \cdot mat333 + k\_v3\_x\_q4 \cdot mat3333 + k\_v3\_x\_q5 \cdot mat33333)$

$$mat\_sum\_v3\_x := \begin{vmatrix} -0.3528238281 & 0. & 0. & 0. \\ 0. & -0.3528238281 & 0. & 0. \\ 0. & 0. & -0.3528238281 & 0. \\ 0. & 0. & 0. & -0.3528238281 \end{vmatrix} \tag{123}$$

Up to the n-th derivative of dipole function at q=0 (here labeled "k_v3_x_q0" for the zeroth derivative,
"k_v3_x_q1" for the first derivative, etc.) multiplied with the integral of $\langle \varphi\_(harm, v = i) | q$
$^n | \varphi\_(harm, v = j)\rangle$.
$dipintegral\_v3\_x := evalf(evalm(mat\_sum\_v3\_x))$
$dipintegral\_v3\_x := \tag{124}$

$$\begin{bmatrix} -0.3528238281 & 0. & 0. & 0. \\ 0. & -0.3528238281 & 0. & 0. \\ 0. & 0. & -0.3528238281 & 0. \\ 0. & 0. & 0. & -0.3528238281 \end{bmatrix}$$

Make a matrix of the product of the eigenvectors of the lowest energy and the next lowest energy
$coeffprod\_v3 := Eigvect\_state1\_v3 \cdot Eigvect\_state0\_v3$
$coeffprod\_v3 := [[-0.124425084453720, -0.0158631865172871, -0.00184965738870538, \tag{125}$
$\quad -0.00420458296000982],$
$\quad [0.924240282870571, 0.117833120695364, 0.0137394149713160, 0.0312320056793504],$
$\quad [0.332577591715410, 0.0424009386211348, 0.00494397574681217,$
$\quad 0.0112384900612852],$
$\quad [0.0487684627762950, 0.00621758244793066, 0.000724973970530267,$
$\quad 0.00164798801202623]]$

Integral of anharmonic wave functions with dipole vector operator multiplied by its product of
eigenvectors, summed.
This gives the contibrution from the x-dipole vector towards the transition dipole moment.
$x\_TDM\_v3 := add(add(dipintegral\_v3\_x[i,j] \cdot coeffprod\_v3[i,j], j = 1..4), i = 1..4)$

$$x\_TDM\_v3 := -1.69965712511211 \; 10^{-13} \tag{126}$$

#---- Calculating the y−vector transition dipole moment:

$mat\_sum\_v3\_y := evalm(k\_v3\_y\_q0 \cdot mat0 + k\_v3\_y\_q1 \cdot mat3 + k\_v3\_y\_q2 \cdot mat33 + k\_v3\_y\_q3$
    $\cdot mat333 + k\_v3\_y\_q4 \cdot mat3333 + k\_v3\_y\_q5 \cdot mat33333)$

$$mat\_sum\_v3\_y := \begin{bmatrix} 0.5537075358 & 0. & 0. & 0. \\ 0. & 0.5537075358 & 0. & 0. \\ 0. & 0. & 0.5537075358 & 0. \\ 0. & 0. & 0. & 0.5537075358 \end{bmatrix} \tag{127}$$

Up to the n-th derivative of dipole function at q=0 (here labeled "k_v3_y_q0" for the zeroth derivative,
   "k_v3_y_q1" for the first derivative, etc.) multiplied with the integral of $\langle \varphi\_(harm, v=i) | q$
   $\wedge n | \varphi\_(harm, v=j) \rangle$.
$dipintegral\_v3\_y := evalf(evalm(mat\_sum\_v3\_y))$

$$dipintegral\_v3\_y := \begin{bmatrix} 0.5537075358 & 0. & 0. & 0. \\ 0. & 0.5537075358 & 0. & 0. \\ 0. & 0. & 0.5537075358 & 0. \\ 0. & 0. & 0. & 0.5537075358 \end{bmatrix} \tag{128}$$

Make a matrix of the product of the eigenvectors of the lowest energy and the next lowest energy
$coeffprod\_v3 := Eigvect\_state1\_v3 \cdot Eigvect\_state0\_v3$
$coeffprod\_v3 := [[-0.124425084453720, -0.0158631865172871, -0.00184965738870538, \tag{129}$
    $-0.00420458296000982],$
    $[0.924240282870571, 0.117833120695364, 0.0137394149713160, 0.0312320056793504],$
    $[0.332577591715410, 0.0424009386211348, 0.00494397574681217,$
    $0.0112384900612852],$
    $[0.0487684627762950, 0.00621758244793066, 0.000724973970530267,$
    $0.00164798801202623]]$

Integral of anharmonic wave functions with dipole vector operator multiplied by its product of
   eigenvectors, summed.
This gives the contibrution from the y-dipole vector towards the transition dipole moment.
$y\_TDM\_v3 := add(add(dipintegral\_v3\_y[i,j] \cdot coeffprod\_v3[i,j], j=1..4), i=1..4)$
$$y\_TDM\_v3 := 2.66735526895101 \; 10^{-13} \tag{130}$$

Calculate the TOTAL transition dipole moment SQUARED

$Tot\_TDM\_v3\_sqr := (x\_TDM\_v3)^2 + (y\_TDM\_v3)^2$
$$Tot\_TDM\_v3\_sqr := 1.00036184737451 \; 10^{-25} \tag{131}$$

Plug the squared total transition dipole moment into molar absorptivity equation to get the Molar
   Absorptivity of q3
Use the harmonic frequency of q3

$$MolAbs\_v3 := \frac{41.6238 \cdot \left(Tot\_TDM\_v3\_sqr \cdot (2.541765)^2\right) \cdot v3\_anharm\_freq}{16.6054}$$

$$MolAbs\_v3 := 4.62985043703483 \ 10^{-21} \qquad \qquad \textbf{(132)}$$

------------------------------END--

Vita

Harkiran Kaur Dhah was born in Fresno, California to Mohinder and Ravinder Dhah in 1987. She attended Central High School and upon graduating in 2005 attended California State University of Fresno to graduate in 2011 with a bachelor of science in chemistry, a bachelor of science in biomedical physics, and a minor in computer science. While at California State University of Fresno she conducted research in organic synthesis under the mentorship of Dr. Santanu Maitra. In Fall of 2012 she began attendance at University of Tennessee, Knoxville to pursue her Doctorate of Philosophy in Physical Chemistry under the mentorship of Dr. Robert J. Hinde. Harkiran will graduate in Summer of 2018 with hopes to pursue an academic career in teaching.